Advanced Engineering Informatics 61 (2024) 102557

Contents lists available at ScienceDirect

Advanced Engineering Informatics

journal homepage: www.elsevier.com/locate/aei

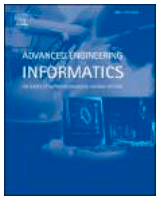

Full length article

Investigating emotional design of the intelligent cockpit based on visual sequence data and improved LSTM

Nanyi Wang, Di Shi, Zengrui Li, Pingting Chen, Xipei Ren *

School of Design and Art, Beijing Institute of Technology, Beijing 100000, China

ARTICLE INFO

Keywords:
New energy vehicles
Intelligent cockpit design
Visual sequence
SSA-LSTM-Attention
Kansei engineering

ABSTRACT

To enhance affective experience and customer satisfaction in the intelligent cockpit of new energy vehicle (NEV-IC), this article proposes a novel method that combines the visual sequence data of eye movements with the sentiment prediction using improved Long Short-Term Memory (LSTM). Specifically, we used eye-tracking technology to capture users' visual sequence of design morphology for NEV-IC. We then adopted entropy-TOPSIS to compute the ranking of morphological components based on experts' opinions, establishing the coupling between users' visual perception and experts' opinion to obtain the key morphological dataset of NEV-IC based on user visual sequence. To tackle the shortcomings of LSTM, meanwhile, we employed the sparrow search algorithm (SSA) to optimize the hyperparameters of the LSTM model. Moreover, an attention mechanism has been introduced to address LSTM's difficulty in preserving key information when processing the sequential data, enabling a stronger focus on critical sequential features within the user's visual path. To assess the efficacy of the proposed SSA-LSTM-Attention model, a dataset incorporating user emotional imagery was constructed, within the research framework of Kansei engineering (KE). This dataset, in conjunction with the morphological dataset of visual sequential features, was applied to our model. The study results indicated that compared to traditional machine learning models like BP neural network (BPNN), support vector regression (SVR), and LSTM, our model performed better in capturing the nonlinear relationship between user sentiment and design features. Additionally, it exhibited higher predictive accuracy, better generalization ability and stronger robustness.

1. Introduction

New energy vehicle (NEV) is generally more eco-friendly than fuel vehicles, which can convert efficiently electricity into the kinetic energy to reduce the overall energy consumption. In recent years, many researchers have begun to pay attention to the design and development of NEV. For example, Nicoletti et al. [1] obtained the design parameters from the analysis of previously constructed model series through the comparison of structured literature, which was used in the early development stage of NEV vehicle design. Lin et al. [2] employed Deep Convolutional Generative Adversarial Network to learn and train the taillight design of NEV, thus building an optimal and creative generative design model. Sun et al. [3] established the NEV framework model through topology optimization and realized the lightweight design of NEV. 8To ensure a pleasant sense of driving, it is essential to capture, connect and satisfy users' emotions for the NEV design [4]. Many NEV manufacturers are prioritizing improvements in both hardware and software, often overlooking the layout of functional components and user interface optimizations. With the integration and optimization of software and hardware in NEV-IC, there is a growing emphasis on intelligent connectivity in the NEV-IC design, including voice assistants, in-car applications, autonomous driving, and vehicle-to-everything services [5]. This has replaced the traditional mechanical features in the cockpits of the cars, thus providing designers with new opportunities to redefine driving experiences [6]. Hence, how to properly capture the emotion of users as well as make the intelligent cockpit design meet the needs for affective driving experiences have become increasingly crucial to the NEV industry [7].

In the research field of emotional design, data-driven techniques such as KE have been widely explored in bridging the relationships between car and user's emotions (e.g., [8,9]). Increasingly, machine learning techniques such as BP neural network [10], interactive genetic algorithm [11], convolutional neural network [12], generative adversarial network [13], have been investigated to fit the nonlinear relationship between users' emotions and design features. Among them, as a novel neural network model, LSTM is good at understanding

* Corresponding author.
E-mail address: x.ren@bit.edu.cn (X. Ren).

https://doi.org/10.1016/j.aei.2024.102557
Received 24 December 2023; Received in revised form 2 April 2024; Accepted 15 April 2024
Available online 22 April 2024

Table 1
Algorithms related to emotional design.

Reference	Algorithm	Application	complexity	Linear/Nonlinear	Loss rate	Fuzzy expression
Su et al. [12]	CNN	Interface interaction	High	Nonlinear	High	High
Wang et al. [24]	BPNN	Electric bicycle	High	Nonlinear	Moderate	High
Kang and Nagasawa. [11]	IGA	Cultural l and creative product	Moderate	Nonlinear	High	Moderate
Kang [8]	SVR	Vehicle	High	Nonlinear	Low	High
Yang et al. [25]	QFD	Nursing bed	Low	Linear	Low	Low
Quan et al. [26]	GRA	Drill	Moderate	Nonlinear	Low	Moderate
Kang [27]	FQFD	Blender	Low	Nonlinear	Low	Moderate
Sheng et al. [28]	AHP	Colors of warship	Low	Linear	Low	Low
Wang and Zhou. [29]	FAHP	Bicycle	Low	Linear	Low	Moderate

information in sequences, which makes it a powerful tool to process sequence data to understand the context [14,15]. Recently, LSTM models have been leverages for a variety of purposes, such as text mining [16], traffic flow prediction [17], visual images [18], bioinformation [19], etc.

For the emotional design of the NEV cockpit, incorporating the user's visual gaze in the design morphology could assist designers in identifying pivotal factors and making improvements [20]. In addition, by inputting morphological data with visual sequence features into the LSTM network, the dependencies between morphology and sequence could be learned, leading to improved understanding over the influence of different morphological components in the overall design. However, the LSTM network still has its blindness and uncertainty in parameter selection, like traditional neural network [21]. To tackle such an issue, Sparrow Search Algorithm (SSA) might be adopted to automatically optimize the initial weight, learning rate and other hyperparameters of LSTM network model [22]. At the same time, adding an Attention mechanism, involving the allocation of weight proportions, to LSTM facilitate the understanding of contextual relationships within the dataset of visual sequence [23]. As a result, an integrated SSA-LSTM-Attention model could be developed, to improve the accuracy of coupling between NEV-IC design features and user emotions.

The contributions of this paper are as follows: (1) In order to better predict users' emotions, this paper proposed an improved LSTM model to increase the prediction accuracy. (2) To enhance the effectiveness of LSTM in utilizing spatial structural information, this paper proposed a data collection method for a design morphological dataset with the visual sequence. (3) The research method proposed in this study produces a set of NEV-IC design, which can provide references for related product design research and practices.

The remaining parts of this paper are organized as follows: In Chapter 2, we showed the details of the proposed method in this study. In Chapter 3, the NEV-IC design process of was put forward and the design results were shown as well. In Chapter 4, the author discussed the comparison between the improvement method proposed in this paper and other relevant methods, and evaluated and verifies the design results produced in this study with other cases. In chapter 5, the author summarized the innovation contribution and shortcomings of the paper, and also provides some suggestions for future research.

2. Related methods

2.1. Related technologies of emotioanl design

As a significant direction in emotional design, KE emphasizes the emotional factors in product design. This includes the affective experience of the user, the affective expression of the product, and the emotional connection between the user and the product. By incorporating emotional elements into the fuzzy front-end development of products, we can create products that are more attractive and arouse users' emotional resonance. How to link product form with user emotions has long been a focal point and challenge in the field of emotional design. It required designers not only to comprehend and apply principles of functionality and aesthetics but also to delve into users' psychological and emotional needs. Additionally, designers needed to master advanced methods and technologies for capturing and measuring user emotions. In order to narrow the gap, many scholars have begun to try to use different methods and techniques to connect the user's emotions and design form. For example, Su et al. [12] proposed a convolutional neural network (CNN)-based architecture for automatic evaluation and labeling of product sentiment, which employs CNN and regression methods to assess the sentiment attributes of products. Wang et al. [24] used BP neural network (BPNN) to identify the relationship between design variables and user emotions to construct a prediction model. Kang and Nagasawa. [11] utilized an interactive genetic algorithm to develop a design system for the evolution of product forms. They translated cultural symbols within products into design forms that resonated with user emotions. Table 1 summarizes the research methods and techniques related to emotional design. However, linear techniques for connecting users' emotions often limited expressive power and are difficult to use when dealing with highly complex or unstructured data. Nonlinear techniques (machine learning, deep learning) often involved complex training and parameter tuning processes, making them prone to overfitting, and lacking the ability to handle sequential data in most cases. As a result, this study proposed a method for gathering the dataset of key morphology with visual sequence features, along with enhancing LSTM-based emotion prediction techniques.

2.2. Methodology for constructing the dataset of key design elements with visual sequence features

2.2.1. Eye-tracking technology

Eye-tracking technology, as a non-invasive experimental tool, has garnered widespread attention in fields such as cognitive psychology, human–computer interaction, and product design [30,31]. The core of eye-tracking technology lies in utilizing specialized equipment to track the movement trajectory of a subject's eyes, in order to understand their visual attention allocation and cognitive processing during observation tasks [32,33]. Accurately recording parameters such as the gaze points, blink rate, and scan paths of the eyes can infer the subject's level of attention to visual stimuli, the depth of information processing, and the thought paths during decision-making processes [34]. The analysis helps unravel individual visual attention patterns and cognitive activities in specific tasks or contexts. Eye-tracking technology can be employed to assess attention allocation and satisfaction during user-product interactions, offering designers profound insights into user emotional preferences for improved and optimized designs. This non-invasive technology, requiring only the participants to wear an eye-tracking device, allows for natural observation tasks without affecting the authenticity of their behavior or cognitive processes. Simultaneously, eye-tracking technology possesses high temporal and spatial resolution, enabling the capture of eye movements and fixation points at the millisecond level. In recent years, eye-tracking technology has been extensively applied in product design. For instance, researchers like Ilhan and Togay [35] utilized eye-tracking technology to study the impact of different details in products on user satisfaction. The research

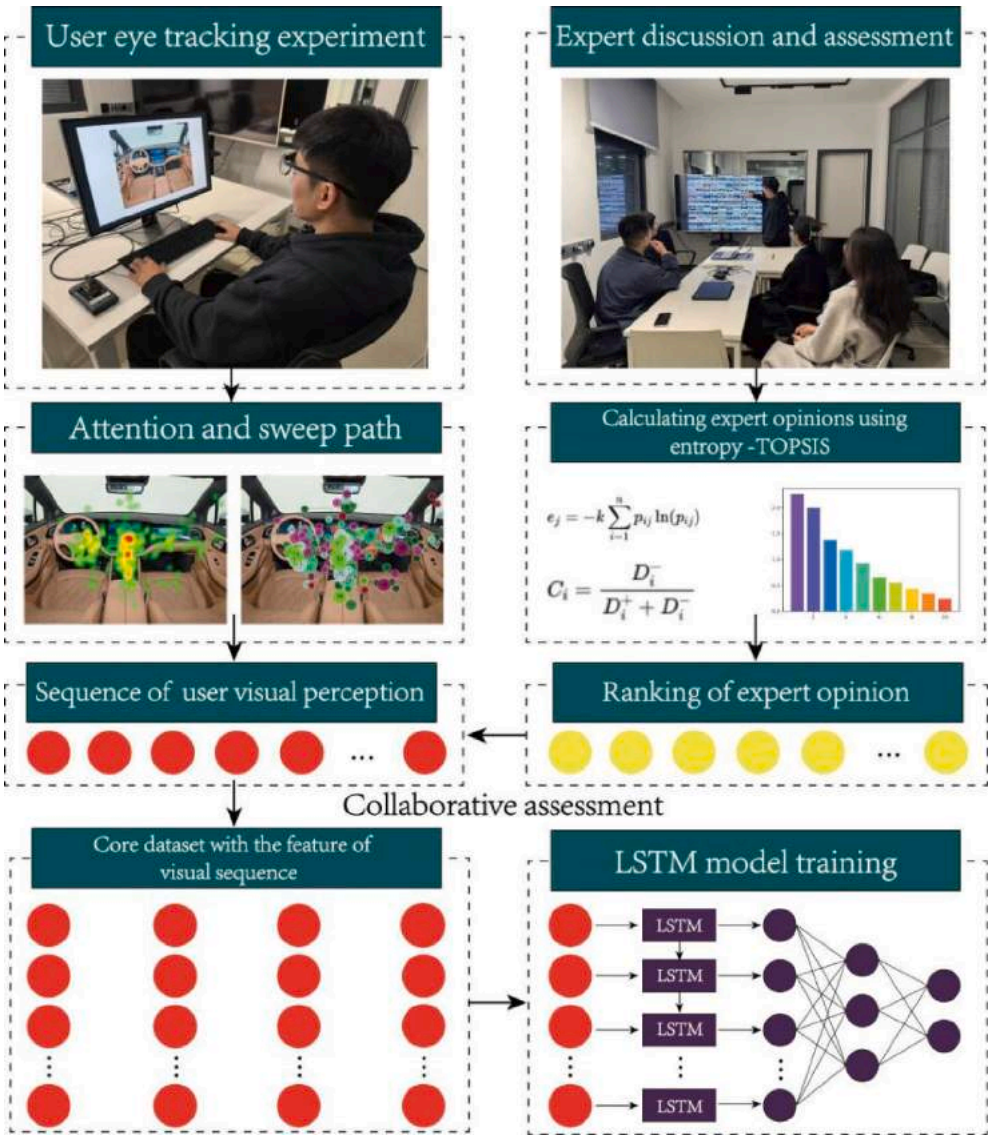

Fig. 1. Method for collecting data of visual sequence.

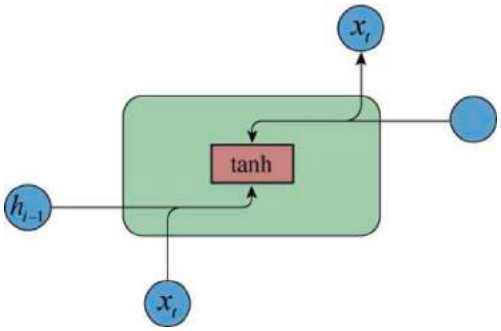

Fig. 2. RNN unit structure.

also elucidated which metrics within eye-tracking technology could be applied to product design and how to judiciously utilize these metrics. Wang et al. [36] utilized eye-tracking technology to forecast decision-making in product design. By integrating EEG signals, a design decision classifier was developed to enhance the scientific and objective nature of decision-making processes. Hsiao et al. [37] proposed a method utilizing eye-tracking to analyze user-object interactions within the 3D navigation space. This approach aimed to comprehend user behavior in VR environments, offering valuable insights for the design of related interactions. In addition, eye-tracking technology finds wide-ranging applications in fields such as architectural engineering [38], aviation safety [39], and biomedical sciences [40].

In the process of product design, understanding users' visual sequence is crucial for optimizing interface layout, product design, and enhancing user affective experience. Eye-tracking technology can capture users' eye movement trajectories when observing samples of NEV-IC, revealing fixation points, scanning paths, and changes in visual attention. This enables analysis of users' attention biases and visual search strategies during observation. However, users are often attracted to design elements that are distinctive, colorful, or prominently placed, and their visual attention is influenced by factors such as personal interests, past experiences, and current task objectives. As a result, a higher perceptual sequence in vision does not necessarily signify a greater importance of these design elements in usage. Therefore, it is important to integrate expert evaluation methods with users' visual perception to deeply understand the design morphology of NEV-IC. This integration offers a more comprehensive and effective approach to collecting data of visual sequence.

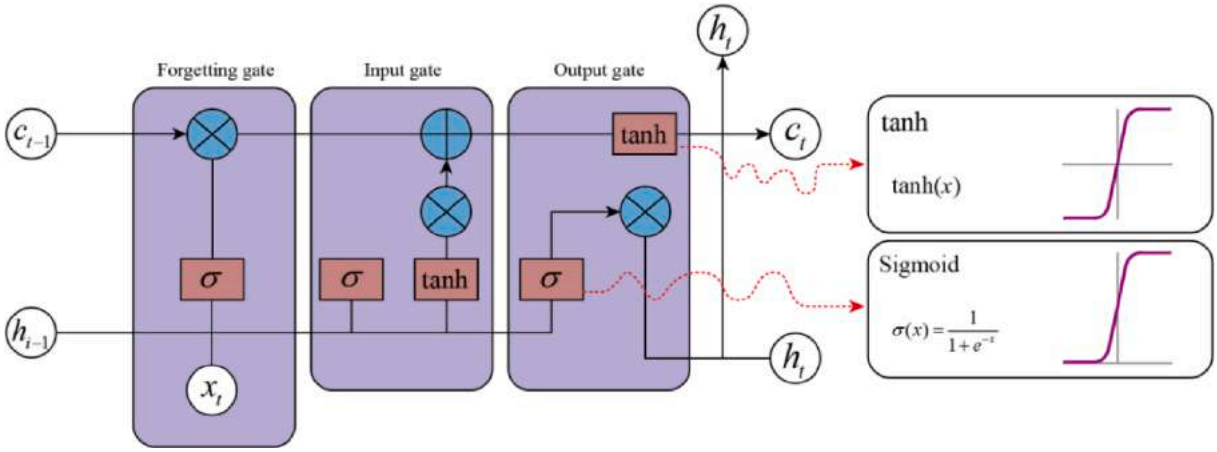

Fig. 3. LSTM unit structure.

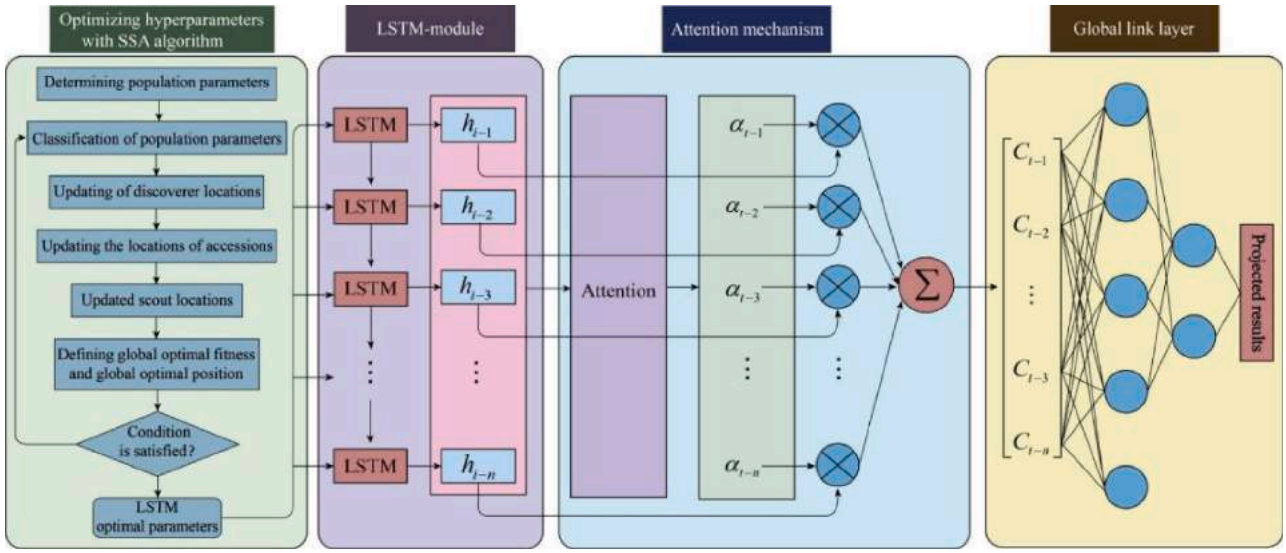

Fig. 4. SSA-LSTM-Attention model structure.

2.2.2. *Entropy-TOPSIS*

Entropy-TOPSIS is a scientific and precise method for comprehensive evaluation, combining entropy weighting with TOPSIS [41]. Entropy weighting is an objective valuation method that helps reduce bias from subjective evaluations. The primary objective is to apply weighting to the indicator system. A larger entropy value indicates greater system disorder, implying less information contained within the sample. Therefore, the weight assigned is smaller accordingly. Conversely, smaller entropy value indicate a more orderly system with more information carried, resulting in larger weights. TOPSIS method evaluates the superiority of each sample by approximating the degree to the ideal solution [42]. In the normalized original data matrix, it identifies the best and worst solutions among finite options. Then, it calculates the distances between the evaluation objects and the best and worst solutions to assess the quality of the samples based on these distances. The specific steps are as follows.

Creating a mean evaluation matrix. The mean matrix is normalized to obtain a standardized matrix; the proportion p_{ij} of No.i evaluation point in the No.j index is calculated, as shown in Formula (1).

$$p_{ij} = \frac{x_{ij}}{\sum_{i=1}^{n} x_{ij}} \tag{1}$$

Calculating the entropy of each indicator. In the formula (2),k is related to the sample size, $k = \frac{1}{\ln n}$; when $p_{ij} = 0$, $p_{ij}\ln p_{ij=0}$; the information entropy of No.j component is calculated as follows:

$$e_j = -k\sum_{i=1}^{n} p_{ij}\ln p_{ij} (j = 1, 2, 3\cdots, m) \tag{2}$$

If the weight coefficient and entropy weight coefficient of each index h_j are greater, the information contained in the component index will be greater and the effect on the evaluation system will be greater accordingly. The calculation formula of the weight coefficient is shown in Formula (3).

$$h_{ij} = \frac{1 - e_j}{\sum_{k=1}^{m}(1 - e_j)} (j = 1, 2, \cdots, m) \tag{3}$$

Integrating the weight coefficients of each indicator into TOPSIS for ranking based on superiority and inferiority. The component attributes are vector normalized to form the decision matrix z_{ij}, the Cosine Distance measure is used to divide each column element with the column vector, as shown in Formula (4).x_{ij} is the evaluation values of No.i evaluation point by expert in the No.j index. So the normalized standard matrix Z could be obtained.

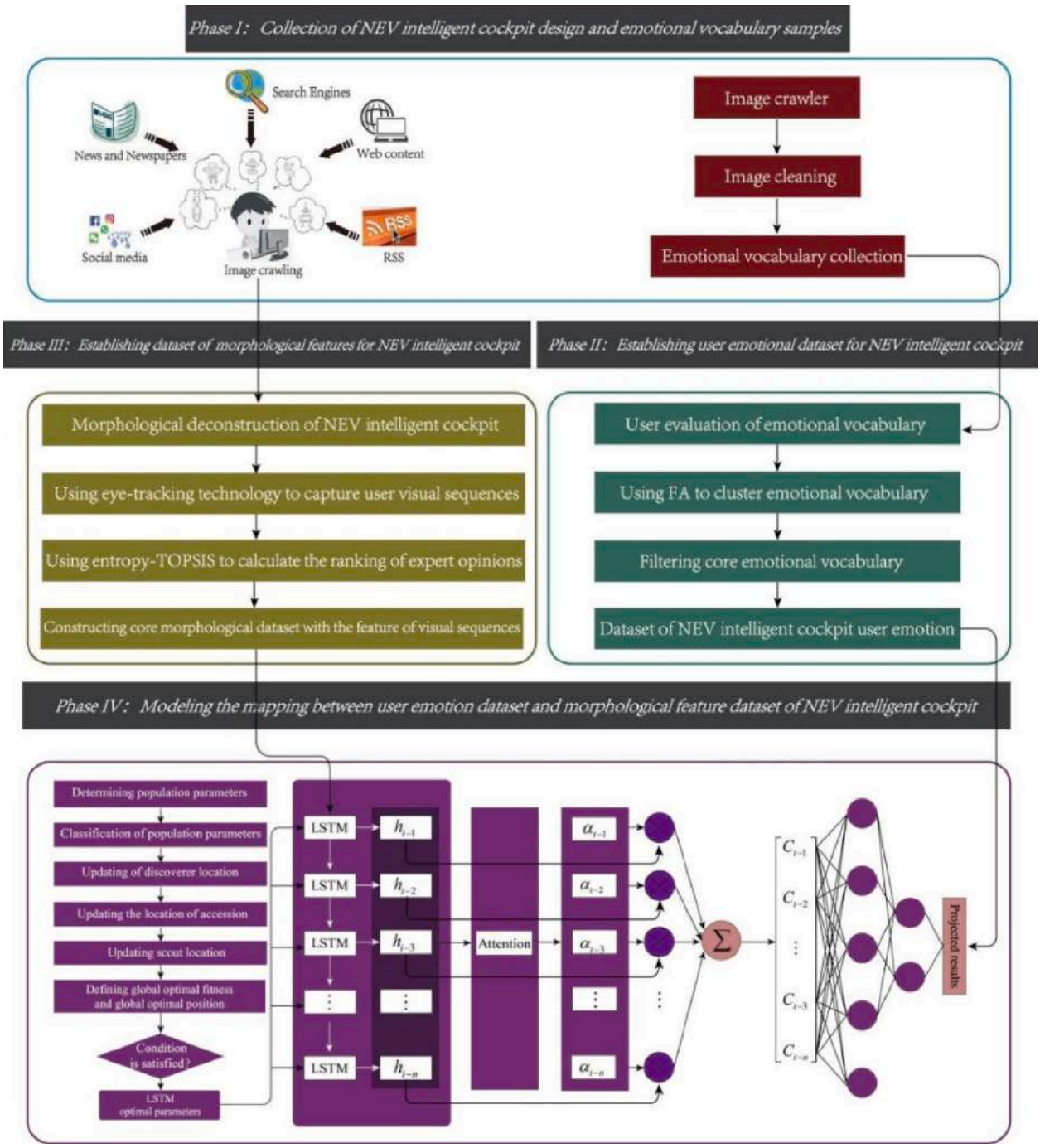

Fig. 5. Design framework of NEV-IC.

$$z_{ij} = \frac{x_{ij}}{\sqrt{\sum_{i=1}^{n} x_{ij}^2}} \tag{4}$$

The positive ideal solution Z^+ and the negative ideal solution Z^- are determined according to each index. The optimal scheme Z^+ is composed of the maximum value of each column in Z, the worst scheme Z^- is composed of the minimum value of each column in Z. The calculation steps are shown in Formulas (5–6).

$$Z^+ = \left\{ \max_{1 \leqslant i \leqslant m} z_{ij} \right\} | J = 1, 2, \cdots, n \} = \{ Z_1^+, Z_2^+, \cdots Z_n^+ \} \tag{5}$$

$$Z^- = \left\{ \min_{1 \leqslant i \leqslant m} z_{ij} \right\} | J = 1, 2, \cdots, n \} = \{ Z_1^-, Z_2^-, \cdots Z_n^- \} \tag{6}$$

Finally, the distance between the optimization index and the optimal scheme and the worst scheme is calculated.w_j is the weight of No.j component.The weighted Euclidean distance between each indicator and the ideal solution is determined. The calculation steps are shown in Formulas (7–9). D_i^+ is the Euclidean distance of the positive ideal solution; D_i^- is the Euclidean distance of the negative ideal solution.

$$D_i^+ = \sqrt{\sum_{j=1}^{m} w_j (Z_j^+ - z_{ij})^2} (i = 1, 2, \cdots, m) \tag{7}$$

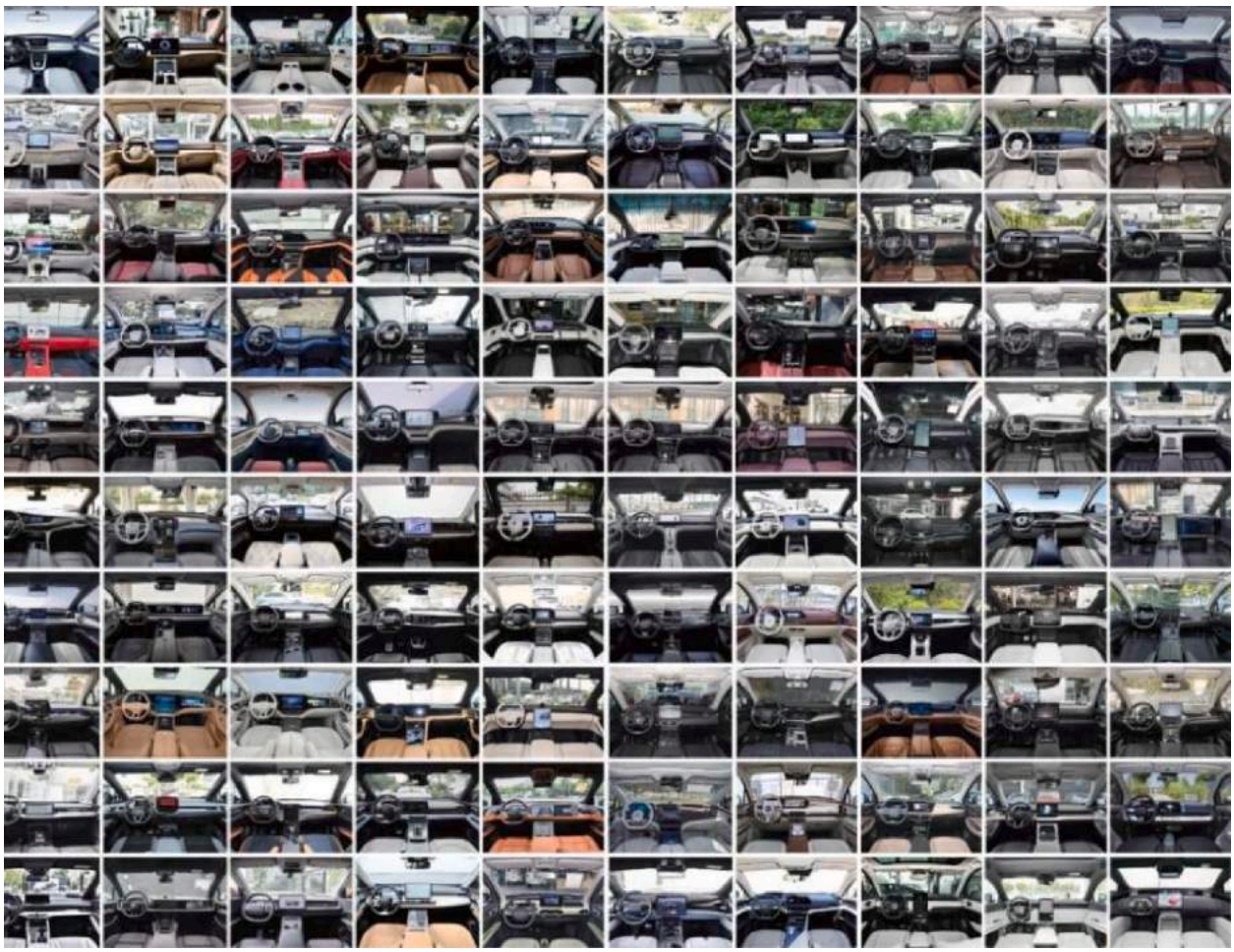

Fig. 6. 100 NEV-IC samples collection.

Table 2
12 emotional vocabulary of NEV-IC.

Simple	Technological	Tidy	Lush	Fashionable	Speedy
Exquisite	Relaxing	Fresh	Brisk	Sturdy	Integral

Table 3
KMO and Bartlett sphericity test.

KMO		0.656
Bartlett sphericity test	Approximate chi-square value	347.569
	Freedom	66
	Significance	<0.001

$$D_i^- = \sqrt{\sum_{j=1}^{m} w_j (Z_j^- - z_{ij})^2} (i = 1, 2, \cdots, m) \tag{8}$$

$$C_i = \frac{D_i^-}{D_i^+ + D_i^-} (i = 1, 2, \cdots, m, 0 \leqslant C_i \leqslant 1) \tag{9}$$

By considering both the relative importance of indicators and the distance between samples and the ideal solution, entropy-TOPSIS offers a more comprehensive evaluation. An increasing number of studies are employing entropy-TOPSIS to rank indicator importance, aiding in decision-making. Huang et al. [43] utilized entropy-TOPSIS to compute and rank indicators for urban rail transit passenger services. This approach provided a comprehensive evaluation of the quality of urban rail transit passenger services, identifying disparities between actual service provision and passenger expectations, with the aim of enhancing travel services for passengers. Wang et al. [44] used entropy-TOPSIS as a universally effective tool for designers in the evolutional design of product forms with multiple objectives. Ouyang et al. [45] improved entropy-TOPSIS to rank the defective quality characteristics of products, addressing the precise measurement of product quality attributes in manufacturing. However, the entropy-TOPSIS method relies on pre-existing data and indicators, making it suitable for expert evaluations

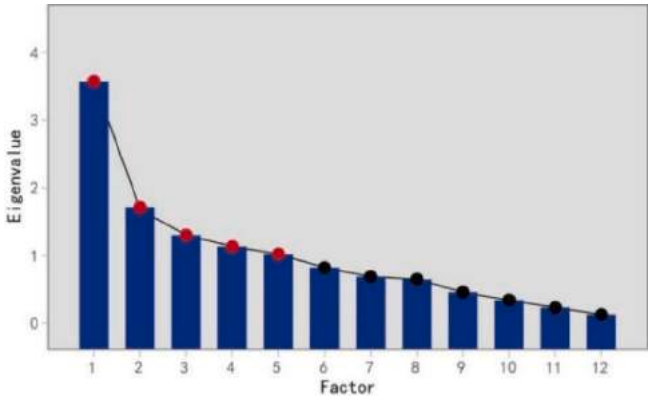

Fig. 7. The scree plot.

Table 4
Total variance explanation.

Initial eigenvalue				Extract the sum of squares			Rotational load sum of squares		
Ingredient	Total	Percentage of variance	Cumulative%	Total	Percentage of variance	Cumulative%	Total	Percentage of variance	Cumulative%
1	3.487	29.058	29.058	3.487	29.058	29.058	2.892	24.103	24.103
2	1.633	13.608	42.666	1.633	13.608	13.608	2.038	16.985	41.088
3	1.315	10.955	53.620	1.315	10.955	10.955	1.349	11.244	52.332
4	1.155	9.623	63.243	1.155	9.623	9.623	1.194	9.948	62.280
5	1.020	8.500	71.743	1.020	8.200	8.500	1.136	9.463	71.743
6	0.822	6.847	78.590						
7	0.700	5.837	84.427						
8	0.631	5.258	89.685						
9	0.452	3.764	93.449						
10	0.316	2.637	96.086						
11	0.260	2.166	98.252						
12	0.210	1.748	100.00						

Table 5
Rotated component matrix.

	1	2	3	4	5
Simple	0.752				
Technological					0.952
Tidy	−0.643				
Lush		−0.795			
Fashionable		0.592			
Speedy	0.799				
Exquisite			0.628		
Relaxing	0.540				
Fresh				−0.905	
Brisk		0.689			
Sturdy			0.813		
Integral	−0.855				

Table 6
User emotional dataset.

Sample	Sense of simplicity	Sense of elegance	Sense of delicacy	Sense of freshness	Sense of technology
1	4.02	4.34	3.14	3.55	4.97
2	3.77	4.05	3.79	3.43	5.55
3	3.55	3.94	4.04	3.92	4.07
4	3.74	4.32	4.02	4.48	5.87
5	5.62	5.08	3.16	5.02	4.77
6	4.22	4.03	4.07	3.72	3.52
7	4.52	4.23	4.22	2.83	5.13
8	3.51	5.55	3.17	3.55	5.43
9	3.92	3.26	3.02	4.96	3.64
10	3.46	5.05	3.73	4.02	3.97
11	4.44	5.02	3.14	4.13	3.56
12	5.32	5.35	3.76	3.74	4.52
13	4.52	5.23	4.06	4.12	3.86
14	4.12	3.14	3.22	5.04	4.37
15	3.84	5.41	4.02	3.67	5.34
16	3.39	4.14	4.36	4.02	4.33
17	4.42	4.43	4.26	3.79	3.89
18	3.87	5.92	3.17	3.22	3.02
19	4.77	3.52	5.07	4.77	4.45
20	4.85	4.77	4.11	3.21	4.26
21	3.91	5.31	3.04	4.41	4.25
22	3.32	4.03	3.47	4.37	4.38
23	4.69	5.63	4.06	4.39	3.93
24	3.97	4.38	3.72	3.55	3.85
25	4.75	4.03	5.43	4.34	4.79
26	3.32	4.07	4.78	3.86	3.96
27	4.82	3.59	5.13	4.69	4.46
28	4.28	4.07	4.18	3.05	4.43
29	4.61	4.45	4.03	3.71	3.59
30	4.52	4.63	2.83	4.15	3.31

regarding the interrelations and relative significance of indicators. This approach is incapable of directly eliciting users' actual perceptual feedback or acquiring users' emotional preferences in real time. This study integrates eye-tracking technology with the entropy-TOPSIS method, employing expert evaluation to assist in the collection of user visual sequence data. Simultaneously, it facilitates a collaborative assessment between users and design experts, exploring the coupling of user visual perception and expert decision-making. It aims to extract component categories of higher importance to enhance computational efficiency, forming an NEV-IC morphological dataset characterized by visual sequence for LSTM model learning and training (Fig. 1).

2.3. SSA-LSTM-Attention

2.3.1. LSTM network

LSTM network is derived from recurrent neural network (RNN) and is mainly used to deal with the problems of time series [46]. In the network architecture of RNNs, the hidden layers are capable of self-connection, and their states can be updated based on the outputs from the previous moment. Therefore, this structure can address the long-term dependency problem in time series (Fig. 2). However, there are certain problems with standard RNN, such as gradient disappearance and gradient explosion, which make it difficult to train long sequential data [47]. LSTM retains the hidden layers of the RNN and introduces a gating mechanism (including forget gate, input gate, and output gate) along with an internal memory cell structure[48,49,50,51]. This architecture addresses the issues of vanishing or exploding gradients when processing time-series data (Fig. 3). The computational steps are detailed in Formulas (10–12). The input weight matrix is represented by W_i^x, W_f^x and W_c^x. b_c, b_i and b_f represent the corresponding deviation. The output fraction at the last moment of the LSTM unit is denoted by h_{i-1}. The input fraction of the time, t is denoted by x_t. tanh represents the hyperbolic tangent activation function in the range (−1, 1) and σ is the sigmoid activation function in the range (0,1).

$$g_t = \tanh(W_c^x x_t + W_c^h h_{t-1} + b_c) \tag{10}$$

$$i_t = \sigma(W_i^x x_t + W_i^h h_{t-1} + b_i) \tag{11}$$

$$f_t = \sigma(W_f^x x_t + W_f^h h_{t-1} + b_f) \tag{12}$$

The calculation formula of the score in the storage unit c_t at point t is shown in Formula (13). In the formula, c_{t-1} represents the memory unit value of last minute.

$$c_t = f_t c_{t-1} + i_t g_t \tag{13}$$

$$o_t = \sigma(W_o^x x_t + W_o^h h_{t-1} + b_o) \tag{14}$$

$$h_t = o_t \tanh(c_t) \tag{15}$$

The score of output gate o_t and the output score of LSTM unit h_t at the time t are calculated in Formulas (14–15). In the formula, W_o^x and W_o^h represent the weight of output gate. b_o represents the deviation matrix

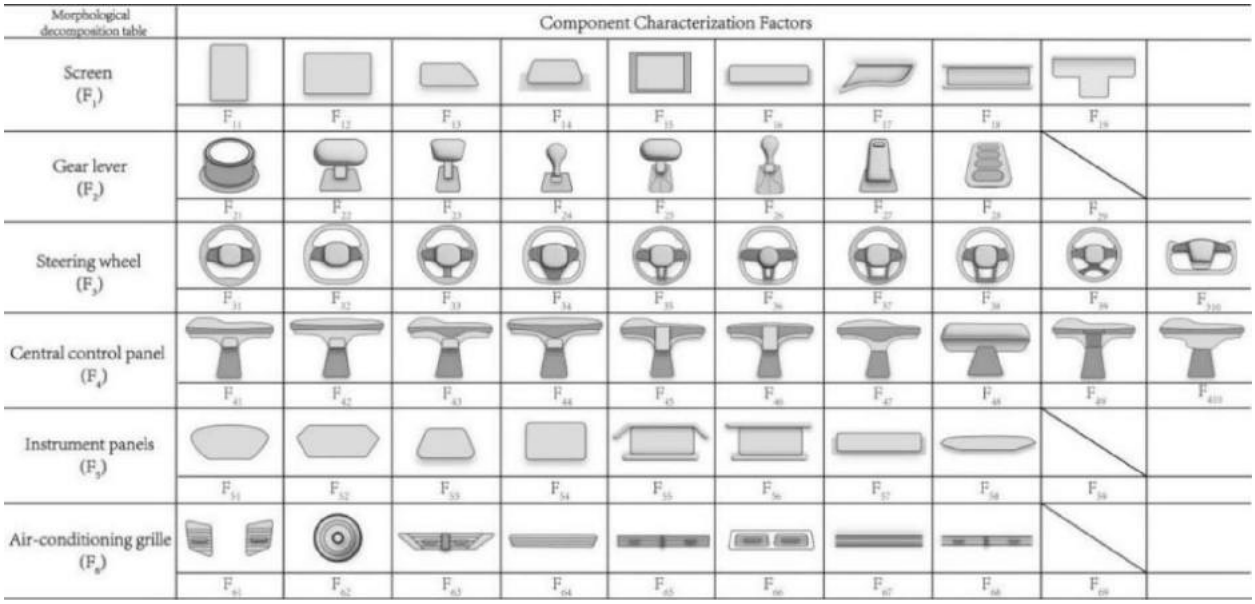

Fig. 8. Morphological deconstruction of NEV-IC.

Table 7
Eye-tracking experiment samples.

	Sense of simplicity	Sense of elegance	Sense of delicacy	Sense of freshness	Sense of technology
Highest score					
lowest score					

and the current output is y_t.

Constructing appropriate activation functions and optimizers aids LSTM in grasping intricate nonlinear relationships, thus enhancing convergence speed. Introducing regularization additionally serves to diminish the risk of LSTM overfitting. Furthermore, the initial value of LSTM weights and biases are generated randomly, the standard gradient descent (SGD) is usually used to update the weights and biases in reverse [52,53]. However, the performance of SGD relies on hyperparameters, such as learning rate and the number of units in the hidden layer. Having more hidden units can aid the model in learning more complex data, but it may also increase training time and resource requirements. The learning rate controls the step size of parameter updates. A smaller learning rate can contribute to stable training but may result in slower convergence, while a larger learning rate might lead to unstable training. Therefore, it is necessary to introduce an optimization method to find the optimal value of hyperparameters, with the aim of enhancing the predictive accuracy of the LSTM model [54].

2.3.2. SSA algorithm

SSA is a new swarm intelligent optimization algorithm, whose principle is to stimulate the foraging and anti-predation behaviors of sparrows by constantly updating individual positions [55,56,57]. In the process of stimulating sparrows, the SSA divides individual sparrows into three possible identities: discoverer (searching for food), participant (following the searcher for food) and scouter (identifying danger) [58,59,60]. Each individual position corresponds to a solution. The three types of individuals constantly update their positions during foraging to obtain resources.

In the simulation test, virtual sparrows are constructed to find objects and the virtual population is represented in Formula (16). In the formula, d is the variable dimension to be optimized.

$$X = \begin{bmatrix} x_1^1 x_1^2 \cdots x_1^d \\ x_2^1 x_2^2 \cdots x_2^d \\ \vdots\vdots\vdots \\ x_n^1 x_n^2 \cdots x_n^d \end{bmatrix} \tag{16}$$

The fitness of all sparrows is expressed in Formula (17); $f(x)$ is the fitness function.

$$X = \begin{bmatrix} f([x_{11} x_{12} \cdots x_{1d}]) \\ f([x_{21} x_{22} \cdots x_{2d}]) \\ \vdots \\ f([x_{n1} x_{n2} \cdots x_{nd}]) \end{bmatrix} \tag{17}$$

The position expression of the discoverer, X_{ij}^{t+1} is shown in Formula (18); in the formula, X_{ij}^{t+1} represents the position of No.i sparrow in the position of j dimension after $t+1$ iteration. α represents a random number in the range of $[0, 1]$; $r_{\max}$ represents the maximum number of

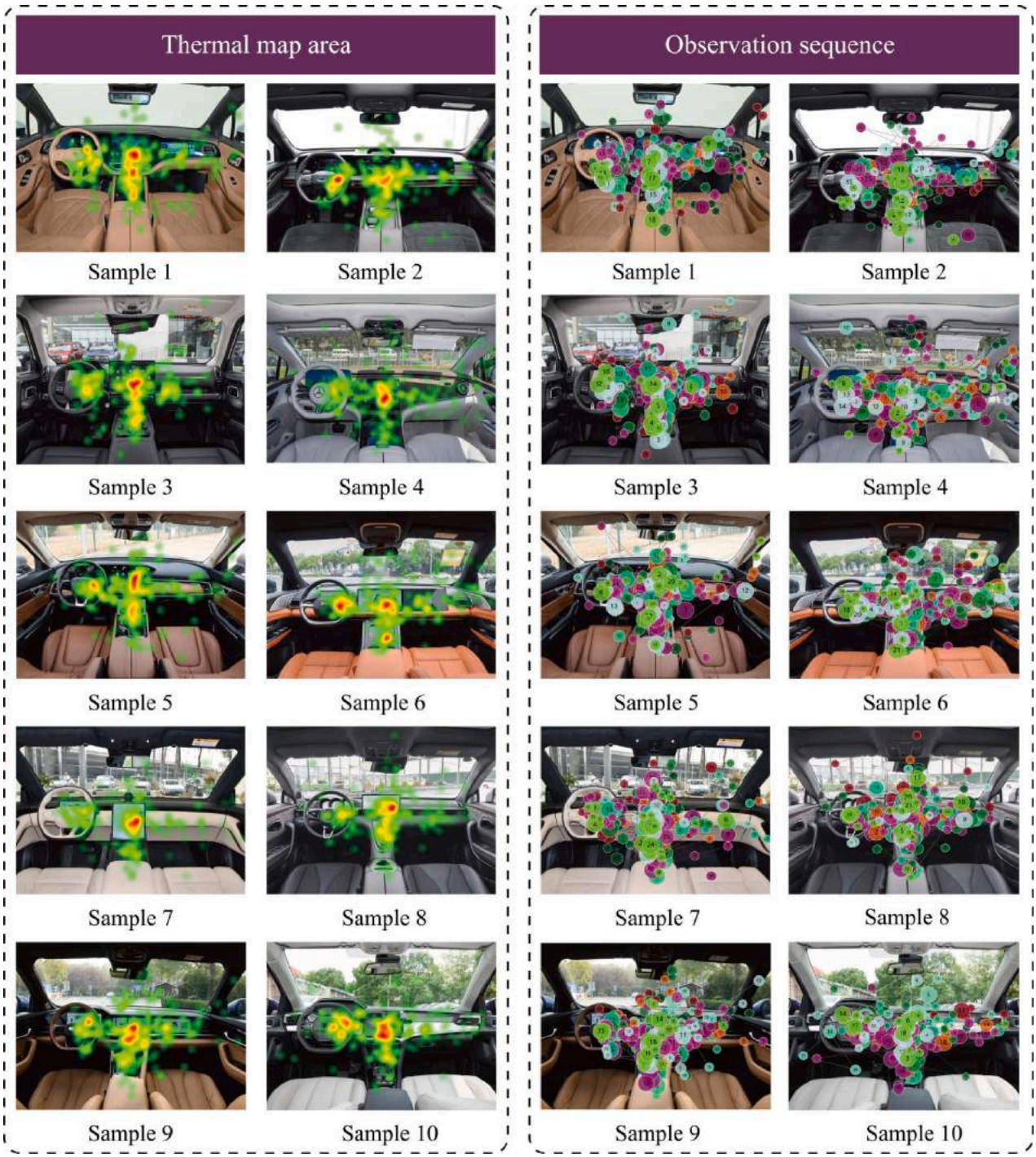

Fig. 9. Heat map and gaze sequence plot of eye-tracking for the NEV-IC.

Table 8
The values of each eye-tracking metric in each AOI region.

	Total fixation duration	Average fixation duration	Fixation count	First fixation duration	Total visit duration	Average visit duration	Visit count
Screen (F1)	1.92	0.40	5.10	0.33	2.16	0.61	3.69
Gear lever (F2)	0.41	0.32	0.85	0.35	0.49	0.39	0.67
Steering wheel (F3)	1.43	0.47	3.67	0.42	1.59	0.71	2.70
Center control panel (F4)	4.85	0.42	12.03	0.443	5.74	1.55	4.68
Instrument panel (F5)	0.64	0.42	1.63	0.42	0.67	0.50	1.34
Air-conditioning grille (F6)	0.54	0.33	1.49	0.32	0.55	0.39	1.34

Table 9
The normalized average values of each component for NEV-IC.

	Total fixation duration	Average fixation duration	Fixation count	First fixation duration	Total visit duration	Average visit duration	Visit count	Average	Sequence
Screen (F1)	0.20	0.17	0.21	0.14	0.19	0.15	0.26	0.19	2
Gear lever (F2)	0.04	0.14	0.03	0.15	0.04	0.09	0.05	0.08	6
Steering wheel (F3)	0.15	0.20	0.15	0.18	0.14	0.17	0.19	0.17	3
Center control panel (F4)	0.50	0.18	0.49	0.19	0.51	0.37	0.32	0.37	1
Instrument panel (F5)	0.08	0.18	0.07	0.18	0.06	0.12	0.09	0.11	4
Air-conditioning grille (F6)	0.06	0.14	0.06	0.14	0.05	0.09	0.09	0.09	5

Table 10
Degree of impact of NEV-IC components on user emotions.

Component category	Sense of simplicity	Sense of elegance	Sense of delicacy	Sense of freshness	Sense of technology
Screen (F1)	5.4	6.2	5.2	4.2	6.6
Gear lever (F2)	5	3.6	3.4	5	2
Steering wheel (F3)	4.6	5.6	5.6	3.6	6
Center control panel (F4)	6.6	6.4	6.2	3.4	7
Instrument panel (F5)	6	5.6	6	2.8	2.4
Air-conditioning grille (F6)	3.4	2.8	3.4	4	2.6

Table 11
Component weighting calculation of NEV-IC.

Category	Information entropy value	Information utility value	Weight value
Sense of simplicity	0.867	0.133	0.14
Sense of elegance	0.850	0.150	0.16
Sense of delicacy	0.766	0.234	0.25
Sense of freshness	0.844	0.156	0.17
Sense of technology	0.734	0.266	0.28

Table 12
Component composite score of NEV-IC.

Component category	positive ideal solution distance (D_i^+)	Negative ideal solution distance (D_i^-)	Composite score index	Sequence
Screen (F1)	0.276	0.779	0.739	2
Gear lever (F2)	0.815	0.458	0.360	5
Steering wheel (F3)	0.392	0.688	0.637	3
Center control panel (F4)	0.297	0.920	0.756	1
Instrument panel (F5)	0.648	0.638	0.496	4
Air-conditioning grille (F6)	0.897	0.231	0.205	6

iterations; Q is a random number which is normally distributed; L is the $L \times d$ matrix where each element is 1; d represents the total size; R^2 indicates the warning value and $R^2 \in [0,1]$;S_T is the safety value and $S_T \in [0.5,1]$.

$$X_{ij}^{t+1} = \begin{cases} x_{ij}\exp(-\dfrac{i}{\alpha r_{\max}})(R_2 < S_T) \\ x_{ij}^t + QL(R_2 \geqslant S_T) \end{cases} \tag{18}$$

As for the participant, the Formula (19) is executed, X_{best}^{t+1} is the global optimal position at the No. t iteration. β is the step size control parameters, which is a normally distributed random number with mean value of 0 and variance of 1. K is a random number in the range of $[-1, 1]$. f_i,f_g and f_w are the current fitness of the sparrow, the global optimal and the worst fitness. ε is a constant to prevent the denominator from being zero.

Fig. 10. NEV-IC morphological components with sequential features.

$$X_{ij}^{t+1} = \begin{cases} X_{best}^t + \beta\left|X_{ij}^t - X_{best}^t\right|(f_i > f_g) \\ X_{ij}^t + K(\dfrac{\left|X_{ij}^t - X_{worst}^t\right|}{f_i - f_w + \varepsilon})(f_i = f_g) \end{cases} \tag{19}$$

At the same time, the Scout is always ready to compete with it, otherwise execute the Formula (20). In this formula, X_p is the optimal position of the discoverer; A is the $1 \times d$ matrix where each element is 1 or -1; and $A^+ = A^T(AAY)^{-1}$.

$$X_{ij}^{t+1} = \begin{cases} Q\exp(\dfrac{x_{worst}^t - x_{ij}^t}{\alpha r_{\max}})(i > \dfrac{n}{2}) \\ X_p^{t+1} + \left|X_{ij}^t - X_p^{t+1}\right|A^+L(i \leqslant \dfrac{n}{2}) \end{cases} \tag{20}$$

Table 13
Feature engineering.

Sample 1	Center control panel (F4)	Screen (F1)	Steering wheel (F3)	Instrument panel (F5)
Serial number	1	2	3	4
Feature encoding	1,0,0,0,0,0,0,0,0,0	0,1,0,0,0,0,0,0,0	0,0,1,0,0,0,0,0,0,0	0,0,0,1,0,0,0,0,0

Table 14
Dataset of morphological characterization.

Sample	Center control pane (F4)	Screen (F1)	Steering wheel (F3)	Instrument panel (F5)
1	1,0,0,0,0,0,0,0,0,0	0,1,0,0,0,0,0,0,0	0,0,1,0,0,0,0,0,0,0	0,0,0,1,0,0,0,0,0
2	1,0,0,0,0,0,0,0,0,0	0,1,0,0,0,0,0,0,0	0,1,0,0,0,0,0,0,0,0	0,0,0,0,1,0,0,0,0
3	0,0,0,0,0,0,0,1,0,0	0,0,0,0,0,1,0,0,0	0,0,0,0,0,0,0,1,0,0	0,0,0,0,0,0,0,0,1
4	1,0,0,0,0,0,0,0,0,0	0,0,0,0,0,0,0,1,0	0,0,0,0,0,0,0,1,0,0	0,0,0,0,1,0,0,0,0
5	0,0,0,1,0,0,0,0,0,0	0,1,0,0,0,0,0,0,0	0,0,0,0,0,0,0,1,0,0	0,0,0,1,0,0,0,0,0
6	0,0,0,0,0,0,1,0,0,0	0,0,0,0,0,1,0,0,0	0,0,0,0,0,0,0,0,1,0	0,0,0,0,0,0,1,0,0
7	1,0,0,0,0,0,0,0,0,0	0,1,0,0,0,0,0,0,0	0,0,0,0,0,1,0,0,0,0	0,0,0,0,0,1,0,0,0
8	1,0,0,0,0,0,0,0,0,0	0,1,0,0,0,0,0,0,0	0,0,0,0,0,0,0,1,0,0	0,1,0,0,0,0,0,0,0
9	0,0,0,0,0,0,0,1,0,0	0,0,0,0,0,1,0,0,0	0,1,0,0,0,0,0,0,0,0	0,0,0,1,0,0,0,0,0
10	0,0,0,0,0,0,0,0,0,1	0,0,0,0,1,0,0,0,0	0,0,0,0,0,0,0,1,0,0	0,1,0,0,0,0,0,0,0
11	0,0,0,0,0,0,0,1,0,0	0,1,0,0,0,0,0,0,0	0,0,0,1,0,0,0,0,0,0	0,0,0,0,0,0,0,0,1
12	0,0,0,1,0,0,0,0,0,0	0,1,0,0,0,0,0,0,0	0,1,0,0,0,0,0,0,0,0	0,0,0,0,1,0,0,0,0
13	0,0,0,0,0,0,0,0,1,0	0,0,0,0,0,0,1,0,0	0,0,0,0,0,1,0,0,0,0	1,0,0,0,0,0,0,0,0
14	0,0,0,0,0,1,0,0,0,0	1,0,0,0,0,0,0,0,0	0,0,0,0,0,0,1,0,0,0	0,0,0,1,0,0,0,0,0
15	1,0,0,0,0,0,0,0,0,0	0,1,0,0,0,0,0,0,0	0,0,0,0,0,0,0,1,0,0	0,1,0,0,0,0,0,0,0
16	0,0,1,0,0,0,0,0,0,0	0,1,0,0,0,0,0,0,0	0,0,0,0,0,1,0,0,0,0	1,0,0,0,0,0,0,0,0
17	0,0,0,0,0,0,1,0,0,0	0,0,0,0,0,1,0,0,0	0,0,0,0,0,0,0,1,0,0	0,0,0,0,0,0,1,0,0
18	0,0,0,0,0,0,0,0,1,0	0,0,0,0,1,0,0,0,0	0,1,0,0,0,0,0,0,0,0	0,1,0,0,0,0,0,0,0
19	0,0,0,0,0,0,1,0,0,0	0,0,0,0,0,0,0,1,0	0,0,0,0,0,1,0,0,0,0	0,0,0,0,0,1,0,0,0
20	0,1,0,0,0,0,0,0,0,0	0,1,0,0,0,0,0,0,0	0,0,0,0,0,0,0,1,0,0	0,0,0,0,0,1,0,0,0
21	0,1,0,0,0,0,0,0,0,0	0,1,0,0,0,0,0,0,0	0,0,0,0,0,1,0,0,0,0	0,0,0,0,1,0,0,0,0
22	0,0,0,0,1,0,0,0,0,0	1,0,0,0,0,0,0,0,0	0,0,0,0,0,0,1,0,0,0	1,0,0,0,0,0,0,0,0
23	0,0,0,0,0,0,0,0,1,0	0,0,1,0,0,0,0,0,0	0,0,0,0,0,0,0,1,0,0	0,0,0,0,0,0,0,1,0
24	0,0,0,0,0,0,0,1,0,0	0,0,0,0,0,1,0,0,0	0,1,0,0,0,0,0,0,0,0	0,0,0,0,0,0,1,0,0
25	0,0,0,0,0,0,1,0,0,0	0,0,0,0,0,0,0,1,0	0,0,0,0,0,0,0,1,0,0	0,0,0,0,0,1,0,0,0
26	0,0,1,0,0,0,0,0,0,0	0,1,0,0,0,0,0,0,0	0,0,0,0,0,0,0,0,0,1	0,0,0,0,1,0,0,0,0
27	0,0,0,0,0,0,1,0,0,0	0,0,0,0,0,0,0,1,0	0,0,0,0,0,1,0,0,0,0	0,0,0,0,0,1,0,0,0
28	0,0,0,0,0,0,0,0,1,0	1,0,0,0,0,0,0,0,0	0,0,1,0,0,0,0,0,0,0	1,0,0,0,0,0,0,0,0
29	0,0,0,0,0,0,1,0,0,0	0,0,0,0,0,1,0,0,0	0,1,0,0,0,0,0,0,0,0	0,0,0,0,0,0,1,0,0
30	0,1,0,0,0,0,0,0,0,0	0,0,1,0,0,0,0,0,0	0,0,0,0,0,0,0,1,0,0	1,0,0,0,0,0,0,0,0

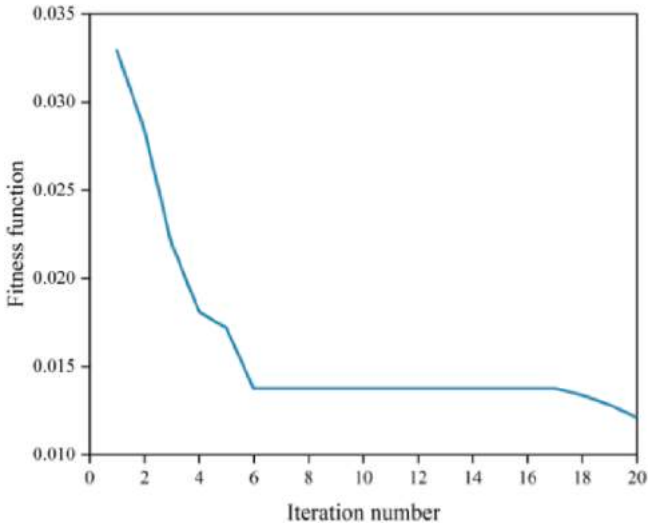

Fig. 11. Convergence curves of SSA.

In the initialization of the model, the SSA algorithm, known for its excellent global optimization capability along with good convergence and stability, is utilized in this study to optimize the hyperparameters of the LSTM model [54].

2.3.3. Attention mechanism

The Attention mechanism is a special structure embedded in the research of machine learning models, which is mainly used for automatic learning and calculating the influence of input data on output data [61–64]. The Attention mechanism can simulate the thinking process of human brain, when processing information, it can pay attention to more important information while ignoring the less important information of the task [65,66]. Therefore, by integrating the Attention mechanism into the LSTM model, it is possible to selectively alter the impact of input feature sequences at different time stages on the prediction results, reasonably allocating features of varying weights. This approach enhances the predictive accuracy of the LSTM model without increasing computational power and storage space requirements [23,67].

The main weight parameters of the Attention mechanism are e_t, t and C_t.. e_t is the weight value corresponding to different features at the time of t. The corresponding calculation formula is Formula (21). In this formula, v and W_e are the weight of multi-layer perceptron when the attention weight is calculate.b_e is the bias of multi-layer perceptron when the attention weight is calculated and h_t is the hidden state vector of the unit output at the time of t.

$$e_t = v\tanh(W_e h_t + b_e) \tag{21}$$

α_t is the weight of attention corresponding to different features at the time of t. In Formula (22), e_j is the weight fraction corresponding to different features at the time of j.

$$\alpha_t = \frac{expe_t}{\sum_{j=1}^{n} e_j} \tag{22}$$

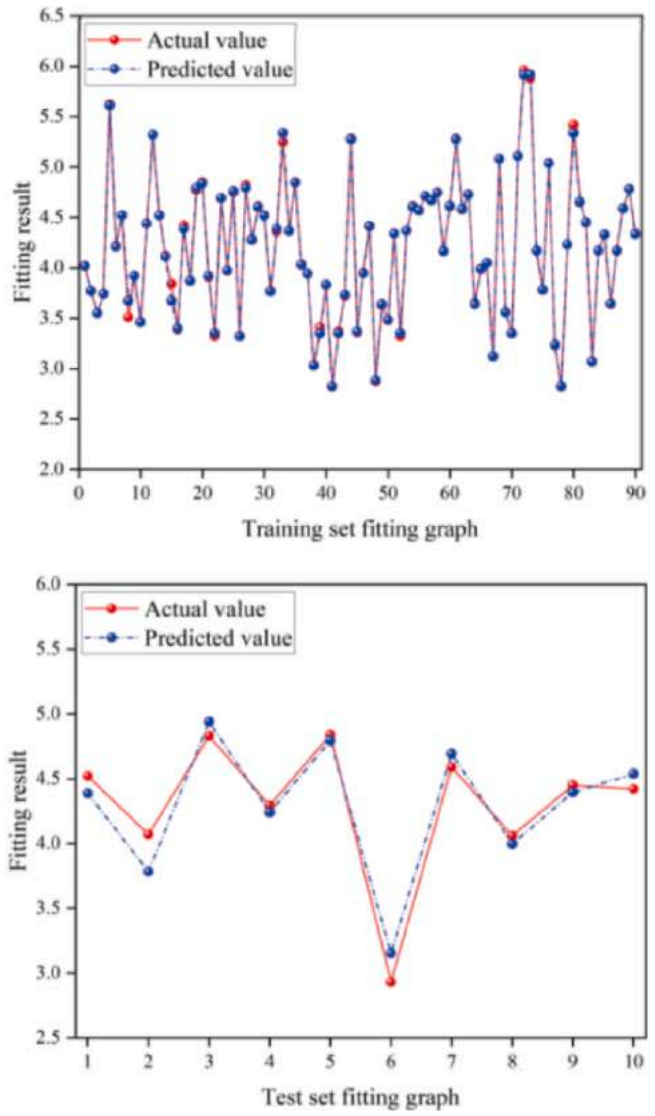

Fig. 12. Fitting plot of "sense of simplicity" dataset.

C_t is the output of the entire attention mechanism at the time of t, which is calculated by Formula (23).

$$C_t = \sum_{j=1}^{n} \alpha_j h_j \tag{23}$$

Utilizing the Attention mechanism to adaptively compute and adjust the hidden layer state values corresponding to the original output features, it focuses on important information, promoting thorough learning and absorption by LSTM. This emphasis on crucial factors uncovers internal connections, thereby enhancing prediction accuracy [68,69]. In the SSA-LSTM-Attention integrated model, the global optimization ability of SSA algorithm is used to optimize the hyperparameters of the traditional LSTM model, reduce the randomness of the model parameter adjustment and improve its flexibility and accuracy. By augmenting the LSTM network with an Attention mechanism, it captures information features outputted by the LSTM layer within the prediction model, allocates weight proportions, and extracts key information. This process enhances the accuracy of NEV-IC user emotion predictions. The specific structure of the SSA-LSTM-Attention integrated model is shown in Fig. 4.

3. Research process and results

3.1. Proposed research framework

The aim of this study is to train a morphological dataset with visual sequence using an improved LSTM, to enhance the accuracy of emotion prediction for users. Additionally, it seeks to construct a mapping model between NEV-IC morphological features and user emotions, thereby designing an NEV-IC that aligns with user emotional imagery. The specific research process is as follows:

Initially, factor analysis (FA) was employed to reduce the dimensionality of collected emotional vocabulary, identifying core vocabulary and establishing an emotional dataset. Next, morphological deconstruction was applied to deconstruct the collected samples of NEV-IC. To obtain a key morphological dataset with visual sequence features, we introduced eye-tracking technology and entropy-TOPSIS to investigate the coupling between experts' opinion and users' perception. The low-influence component categories were eliminated, resulting in the formation of a key morphological dataset with visual sequence features. Finally, the key morphological dataset (feature values) with visual sequence features and the user emotional dataset (target values) are imported together into the SSA-LSTM-Attention model. This constructs a mapping model between user emotional imagery and NEV-IC morphological design. The trained SSA-LSTM-Attention model is then used to predict the optimal morphological combination. The specific research framework is depicted in Fig. 5.

3.2. Sample collection for morphological features and emotional vocabulary of NEV-IC

In this study, the web crawler technology was used to crawl a wide range of image samples from major automotive websites with keywords such as "car interior", "car cabin", and "car interior space". Due to the complexity of the cockpit inside the car, the angle of center console in the NEV-IC was selected as the sample angle in this study. All image samples are from actual user shots. After focus group discussion, the repetitive, unclear, distorted angle images and the images without the features of the NEV-IC were removed. 100 representative image samples of NEV-IC with uniform viewing angles and high resolution (Fig. 6) were selected. Through Internet search and literature references, 50 expressions of users' emotional image representing the NEV-IC were collected and stored in the form of vocabulary. Later, 5 experts with a background in NEV-IC design were invited to screen the 50 emotional words, meaningless words (such as good looking, beautiful), similar or duplicate words (such as technological and technical) were removed. Finally, 12 representative emotional words were selected. The emotional words were randomly sorted and numbered, as shown in Table 2.

3.3. Establishing dataset of emotional design for NEV-IC

3.3.1. Establishment of user emotional dataset for NEV-IC

Factor Analysis (FA) [70,71,72] is a statistical technique commonly used for data reduction and discovering potential structures in data, it can be used for dimensionality reduction of emotional words to aid the emotional design of the NEV-IC. In the emotional design of NEV-IC, a large number of emotional words have potential consistency and express the same emotional characteristics of users. FA can be used to reduce multi-dimensional emotional words to the most concise dimension, as a result, the complex emotional words data can be converted into potential factors that are easier to understand and apply. It can facilitate better understanding and analysis of users' emotions, thus better guiding the design and improvement of NEV-IC. In order to establish the quantitative relationship between users' emotions and sample images, the collected 12 emotional words were distributed to 60 people on a seven-level Likert scale. 100 NEV-IC samples were scored by correlation, 60 users' evaluations were collected, and the emotional evaluation matrix

Fig. 13. Emotional design of NEV-IC.

of NEV-IC was constructed in the form of an average values. In order to reduce the information load and find the potential consistency of each emotional word, FA conducted dimensionality reduction on the matrix data of emotional evaluation.

Through the use of the SPSS software, the KMO value is calculated as $0.656 > 0.5$, the Bartlett sphericity = 347.569 (freedom = 66) and the significance value < 0.001. The results show that this dataset is suitable for FA (Table 3). The scree plot (Fig. 7) and the total variance (Table 4) reveal five components with eigenvalues greater than 1, indicating that the dataset can be reduced to five categories of factors. The cumulative contribution rate of the five factors after reduction reaches 71.743 %. In the component matrix after rotation (Table 5), simple, tidy, speedy, relaxing and integral were classified into one category. Simple, tidy, relaxing and integral express the feeling of simplicity, and speedy also expresses an inherent simplicity to some extent. So factor of this type was named as the sense of simplicity. Lush, fashionable and brisk were classified as one category, which expresses elegance, so it was named as a sense of elegance. Exquisite and sturdy emphasize the characteristics of high quality, tightness and durability, which was named as a sense of delicacy. Fresh and technological were classified into two categories respectively, which were named as the sense of freshness and sense of technology. After extracting the core user emotional vocabulary, it was distributed to 60 people again to evaluate the emotional vocabulary, constructing the NEV-IC user emotional dataset (Table 6). Due to limitations in paper length, the comprehensive emotional dataset is provided in Appendix A1.

3.3.2. Constructing key morphological dataset of NEV-IC with visual sequence features

To obtain a core morphological dataset with visual sequence features, we first conducted morphological classification and deconstruction of NEV-IC. We employed eye-tracking device to capture users' visual paths and utilized entropy-TOPSIS to compute ranking of expert opinion. This approach allows us to investigate the coupling between users' visual perception and experts' opinion. In order to enhance the efficiency and rationality of NEV-IC design and avoid overwhelming data load from excessive morphological categories, we selectively retained key morphological categories that exhibited high consistency with users' visual perception and experts' opinion. This approach resulted in the creation of NEV-IC key morphological dataset with visual sequence features.

3.3.2.1. Establish a morphological deconstruction table for the NEV-IC.

Morphological deconstruction is an important method in KE, which can help designers deeply understand the emotional characteristics of objects and apply them into products design to achieve better user experience and emotional resonance [73]. Designers can compare combinations of different features and attributes in the deconstructed form matrix, they can also better assess the impact of different design decisions. After discussion of focus group, we classifiied six types of NEV-IC morphological categories: screen (F_1), gear lever (F_2), steering wheel (F_3), center control panel (F_4), instrument panel (F_5), air-conditioning grille (F_6). Through in-depth observation of 100 NEV-IC samples, specific features of each morphological category were deconstructed, leading to the establishment of a morphological deconstruction table for NEV-IC (Fig. 8).

3.3.2.2. Utilizing eye-tracking technology to acquire user visual sequence.

To assess user visual perception, we conducted an eye-tracking experiment with 12 users experienced in driving NEV. Heat map regions and observation sequence of users observing the samples of NEV-IC were obtained through the experiment. The experimental design is as follows:

(1) Samples

We selected samples from the user emotional dataset of NEV-IC in Appendix A1 that had the most impact on user emotions. Specifically, we chose the samples with the highest and lowest scores for each emotional category, resulting in a total of ten images, as shown in Table 7. Additionally, we maintained uniform resolution and dimensions for each selected sample.

(2) Participants

We recruited 12 participants with experience in driving NEV for this experiment. No textual cues related to the vehicles were provided before or during the tests to avoid influencing participants' subjective perceptions.

(3) Devices

The equipment utilized comprised Tobii Pro Glasses 2 and a 21-inch computer monitor. The data collection and analysis were facilitated by Tobii Pro Glasses Controller (x64) and Tobii Pro Lab software.

(4) Experiment procedure

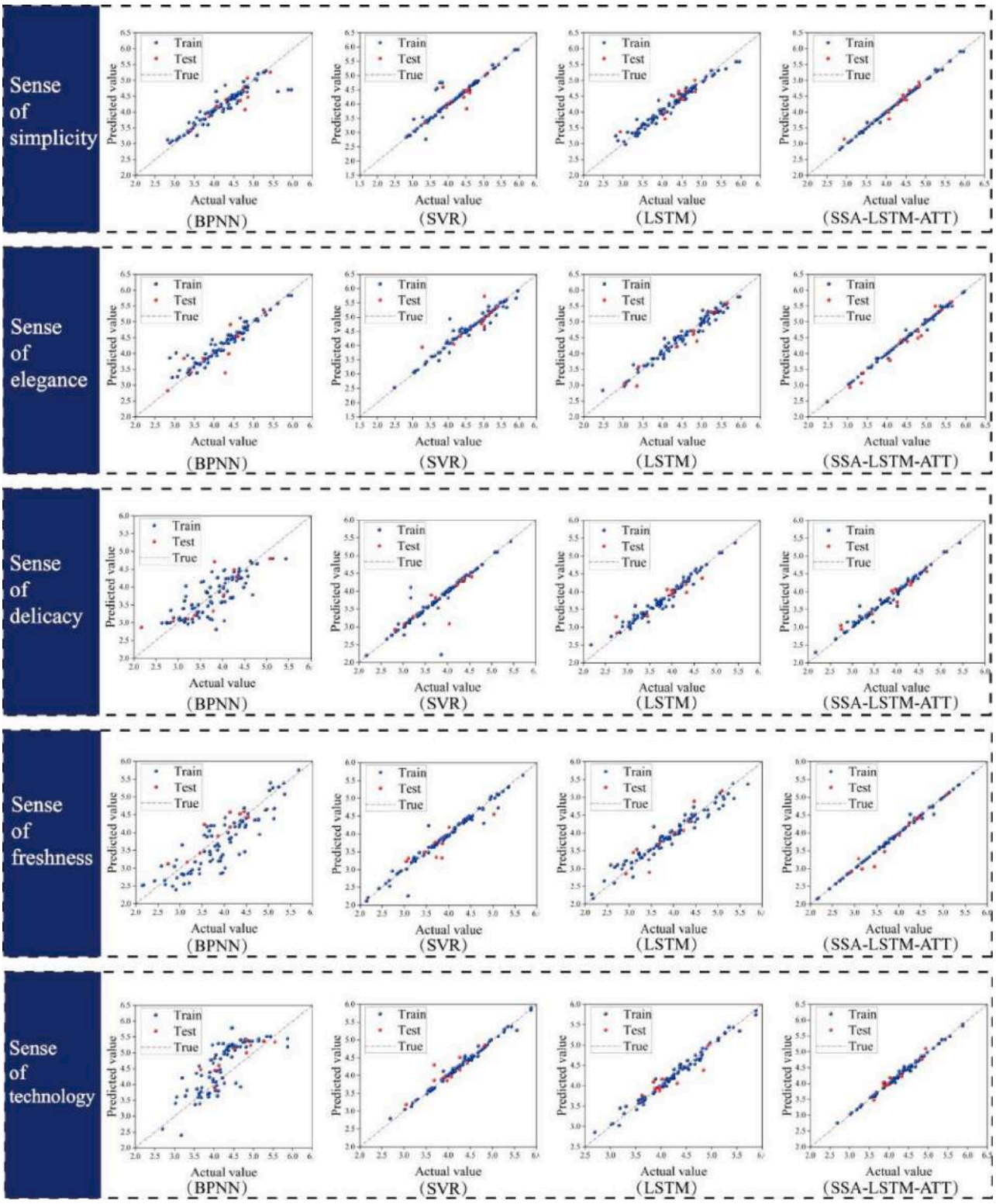

Fig. 14. Comparison of scatter plot: each row represents the performance of four models on the same dataset.

Upon entering the experimental phase, participants were briefed on the procedures and guidelines. After becoming acquainted with the environment, participants were fitted with eye-tracking glasses for device calibration and pre-testing to ensure the accuracy of experimental data. Positioned in front of a 21-inch computer screen, participants focused on the central area and initiated the experiment by clicking the mouse as instructed. Subsequently, the computer screen displayed an image of NEV-IC every 15 s, with each image appearing for 10 s. The experiment concluded after 10 repetitions of this sequence.

After concluding the experiment, we utilized Tobii Pro Lab software to export overlaid user heat map regions and observation sequence for the 10 NEV-ICs. Based on Fig. 9, it is evident that the visual attention of the 12 participants primarily focused on the center control panel, screen, and steering wheel area of the NEV-IC. Similarly, the observation

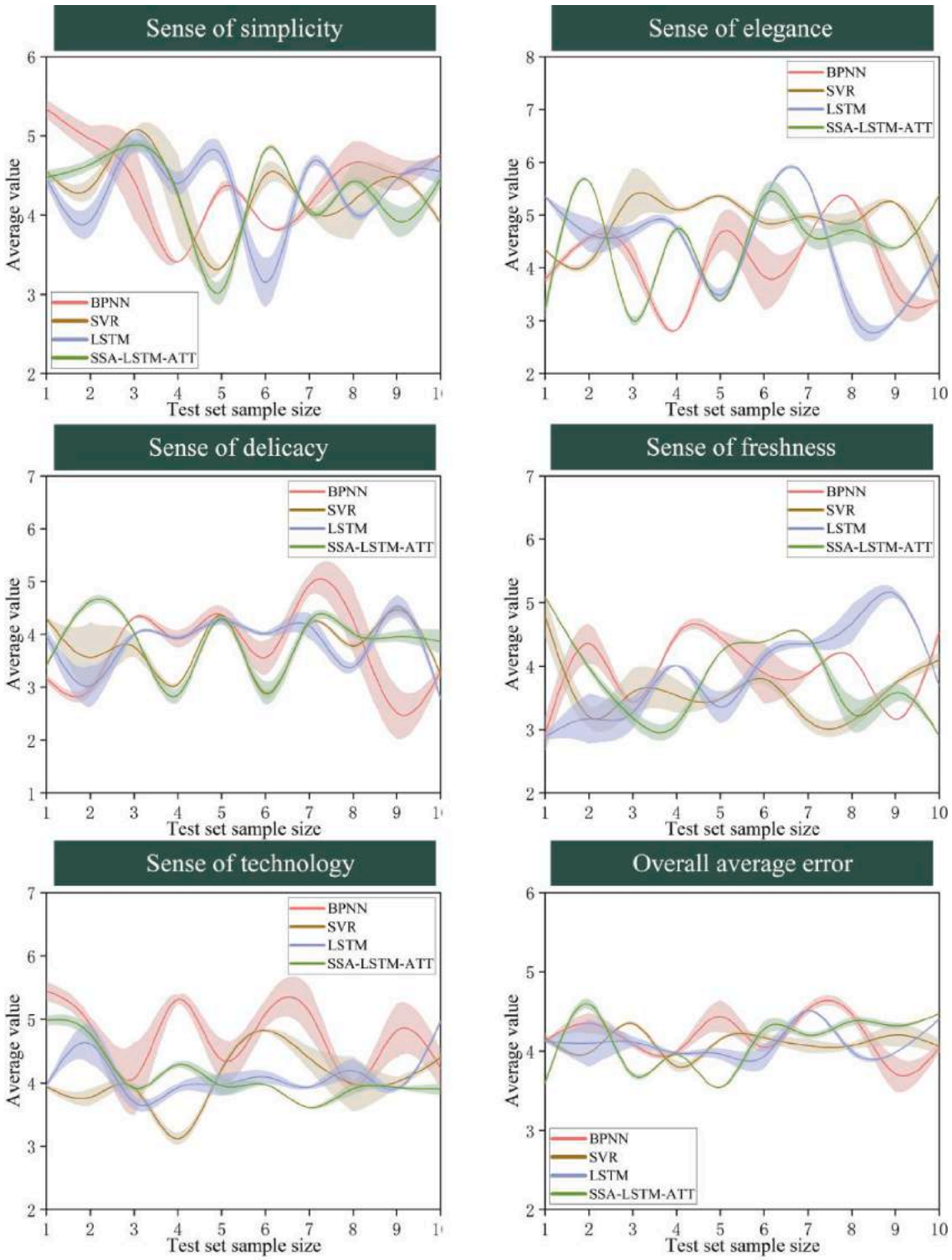

Fig. 15. Comparison of error band diagram.

frequencies and sequences were predominantly concentrated in these regions. Using the classification from Fig. 8, we categorized the samples into 6 distinct AOI regions. Subsequently, we compared and computed the mean values of 7 metrics influencing user visual perception: total fixation duration, average fixation duration, fixation count, first fixation duration, total visit duration, average visit duration, and visit count. These results were summarized in Table 8. We further normalized the values of each metric column to compute the average for each morphological category across all metrics, as shown in Table 9. In comparison, the user visual sequence for the NEV-IC morphological category was as follows: center control panel (F4) > screen (F1) > steering wheel (F3) > instrument panel (F5) > air-conditioning grille (F6) > gear lever (F2).

3.3.2.3. Exploring expert opinion decision making by computing entropy-TOPSIS. We invited five industrial designers with background in NEV-IC design to rate the impact of six morphological categories on user emotions, establishing a mean matrix of seven-level Likert scale (Table 10).

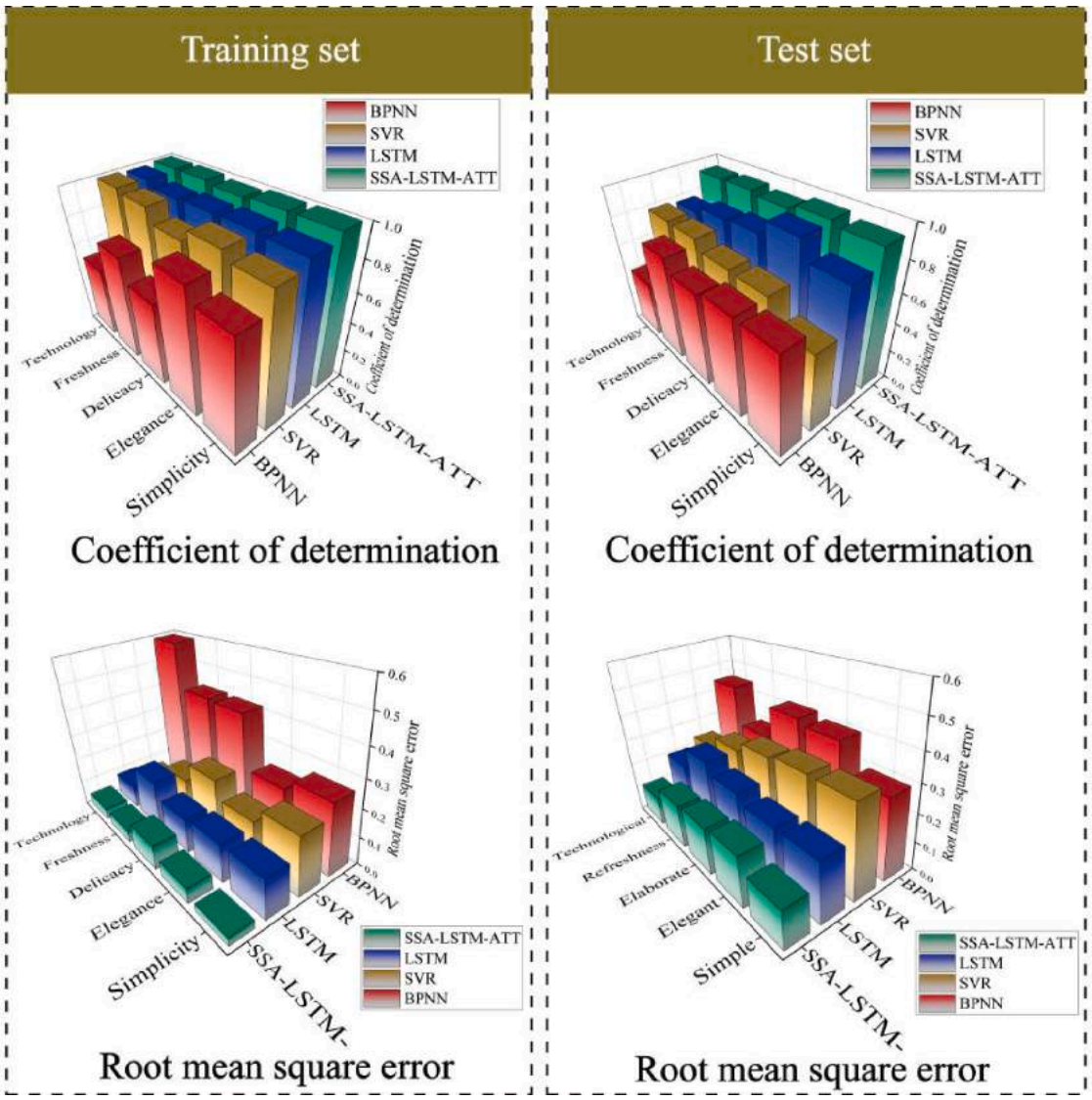

Fig. 16. Comparison of R^2 and RMSE.

Following Formula (1), the mean matrix was normalized to obtain the standardized matrix. Using Formulas (2–3), we calculated the entropy values and weight coefficients of emotional vocabulary for NEV-IC, resulting in the information entropy values, information utility values, and weight values of emotional vocabulary, as shown in Table 11. The weighting coefficients of emotional vocabulary for NEV-IC were integrated into TOPSIS, with a total of six evaluation objects, each having five emotional evaluation attributes. The attributes of each morphological component were vector normalized according to Formula (4) to form a decision matrix. Using Formulas (5–9), we calculated the positive and negative ideal solutions for the morphological categories of NEV-IC, as well as the distances between each indicator and the optimal and worst-case scenarios. According to Table 12, the comprehensive scores for various components of the NEV-IC were ranked as follows: center console (F4) > screen (F1) > steering wheel (F3) > instrument panel (F5) > gear lever (F2) > air-conditioning grille (F6).

3.3.2.4. Creating key morphological datasets with visual sequence features by incorporating expert opinions and user visual perception. Upon comparing the results of eye-tracking and entropy-TOPSIS, we observed a significant agreement between the users' visual perception and the experts' opinions. Specifically, the center control panel (F4) > screen (F1) > steering wheel (F3) > instrument panel (F5) were ranked consistently. These morphological components are considered key and valuable for NEV-IC design. To enhance the efficiency of subsequent design and computation, we retained the most critical 4 morphological components, resulting in the key morphological components with the feature of visual sequence, as shown in Fig. 10.

In order to enable the computer to recognize the sample features, we carried out feature engineering processing on 100 NEV-ICs and encoded them into computer-recognizable features. According to the morphological deconstruction table in Fig. 6, we deconstructed 100 samples in coded form. For example, the screen form of sample 1 is composed of the No.2 form in the morphological deconstruction table, the coding of the sample was recorded as: 0,1,0,0,0,0,0,0,0 (Table 13). Encoding and arranging 100 NEV-IC samples based on visual sequences, we constructed a NEV-IC morphological dataset with visual sequence features (Table 14). Due to limitations in the length of the paper, the complete morphological dataset can be found in Appendix A2.

3.3.3. Modeling the mapping between user emotional dataset and morphological dataset of NEV-IC

The morphological dataset (Table 14), serving as feature values, along with the user emotional evaluation values (Table 6) as target values, are imported into the established SSA-LSTM-Attention model for learning and training. Firstly, we adopted SSA to optimize the initial

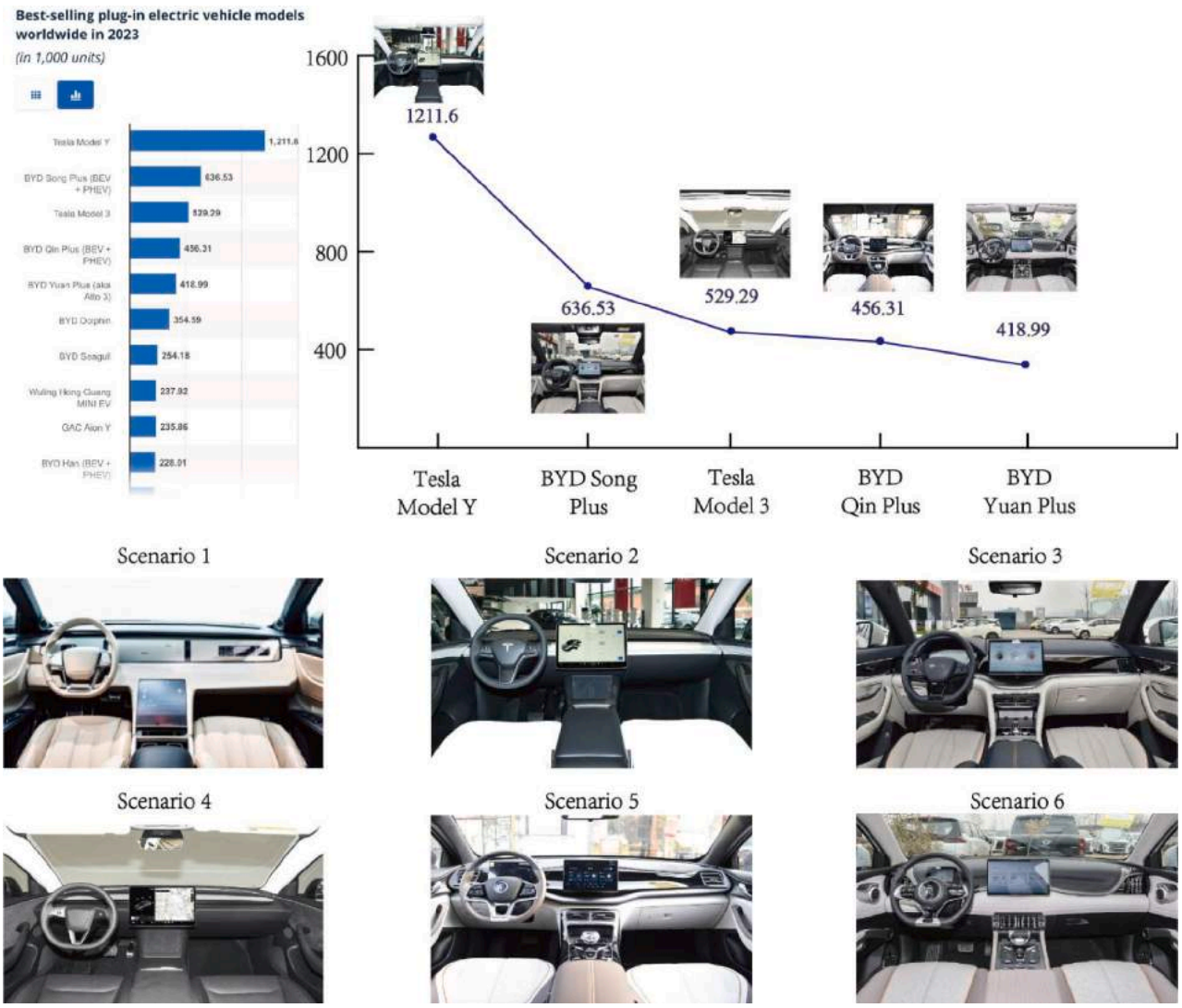

Fig. 17. The NEV-IC design that achieved the highest sales in 2023.

learning rate of LSTM, hidden layer nodes and other hyperparameters. The sparrow population size was set to 30, the number of optimizations was set to 20, and the upper and lower limits of the optimization parameters were set. In the Attention mechanism layer, we incorporated global average pooling layer, RELU activation layer, and sigmoid activation layer, embedding them between the LSTM layer and the full connection layer. At the same time, the coefficient of determination (R^2) and root mean square error (RMSE) were used as evaluation metrics for the prediction accuracy of the model [74,75], as shown in Formulas (24–25). In the formula, n is the number of samples;y_i and $\widehat{y}_i$ represent the actual score and predicted score of the time i;$\widehat{y}$ is the average value of samples in the test set.

$$RMSE = \sqrt{\frac{1}{n}\sum_{i=1}^{n}(\widehat{y}_i - y_i)^2} \tag{24}$$

$$R^2 = 1 - \frac{\sum_{i=1}^{n}(y_i - \widehat{y}_i)^2}{\sum_{i-1}^{n}(y_i - \overline{y}_i)^2} \tag{25}$$

After setting the optimized parameters, we took the "sense of simplicity" dataset as an example. The maximum training times of the LSTM network was set to 2000 times, the learning rate was adjusted after 850 training times, and the activation function was set as RELU function. Fig. 11 shows the convergence curve in the SSA iteration process. Through the optimization and iteration of SSA algorithm and the capture of data features by the Attention mechanism, LSTM was used to establish the mapping relationship between users' emotion (sense of simplicity) and morphological features of NEV-IC. To prevent the model from overfitting, we added an L2 regularization term to the loss function to penalize the weight coefficients of the model, avoiding the model from relying too much on the noise in the training data, thus reducing overfitting. By adding the L2 regularization term, the model minimized not only the RMSE but also the sum of squares of the weights during training. This means that the model needs to find a balance between fitting the data and keeping the weights small, which reduces the prediction error on unseen data and improves the generalization ability of the model. Concurrently, we utilized the Adam optimizer to adjust the learning rate based on the gradient of each parameter, allowing for a faster convergence to better solutions. The Adam optimizer incorporates the concept of momentum, which aids in accelerating the gradient descent process while preserving directionality during parameter updates, thereby leading to a quicker convergence to local optima. The fitting results for the training iterations are shown in Fig. 12, the training set and test set were used to converge the better R^2 (0.998, 0.928), RMSE (0.0303, 0.1405). Its fitting diagram is shown in Fig. 12. The experimental results show that the SSA-LSTM-Attention integrated model has high prediction accuracy and can be used to establish the mapping relationship between users' emotions and morphological features of

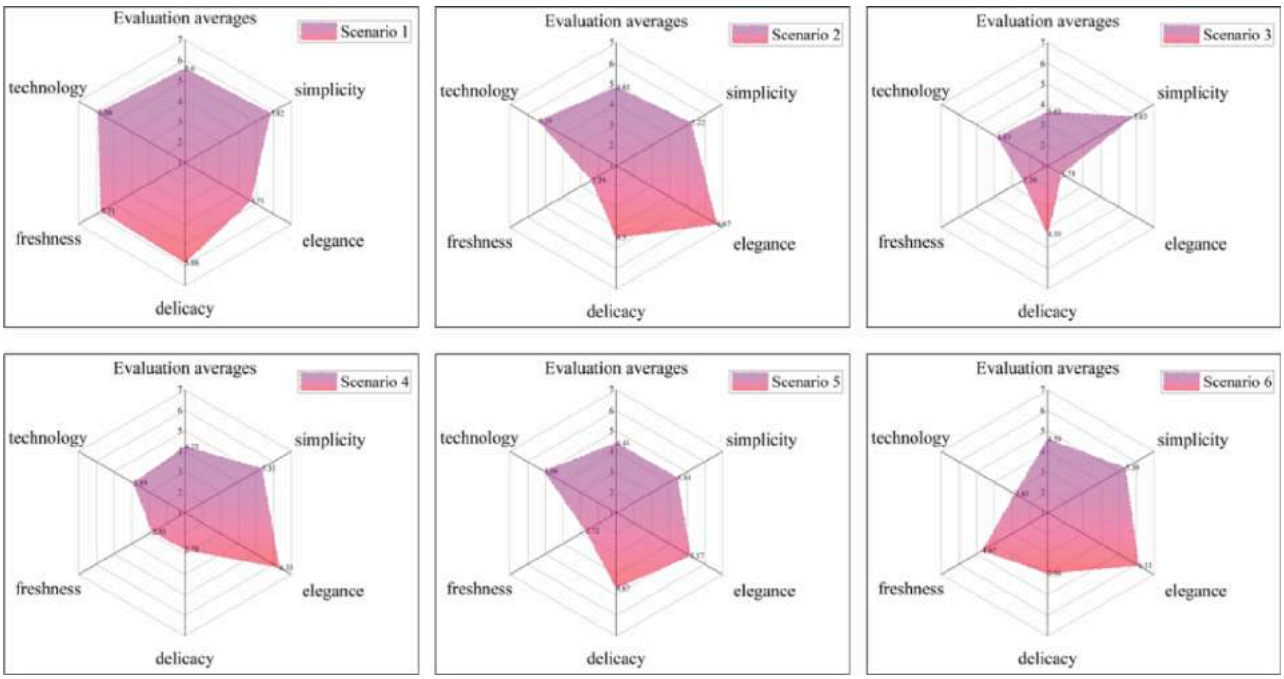

Fig. 18. Evaluation results for 6 NEV-ICs.

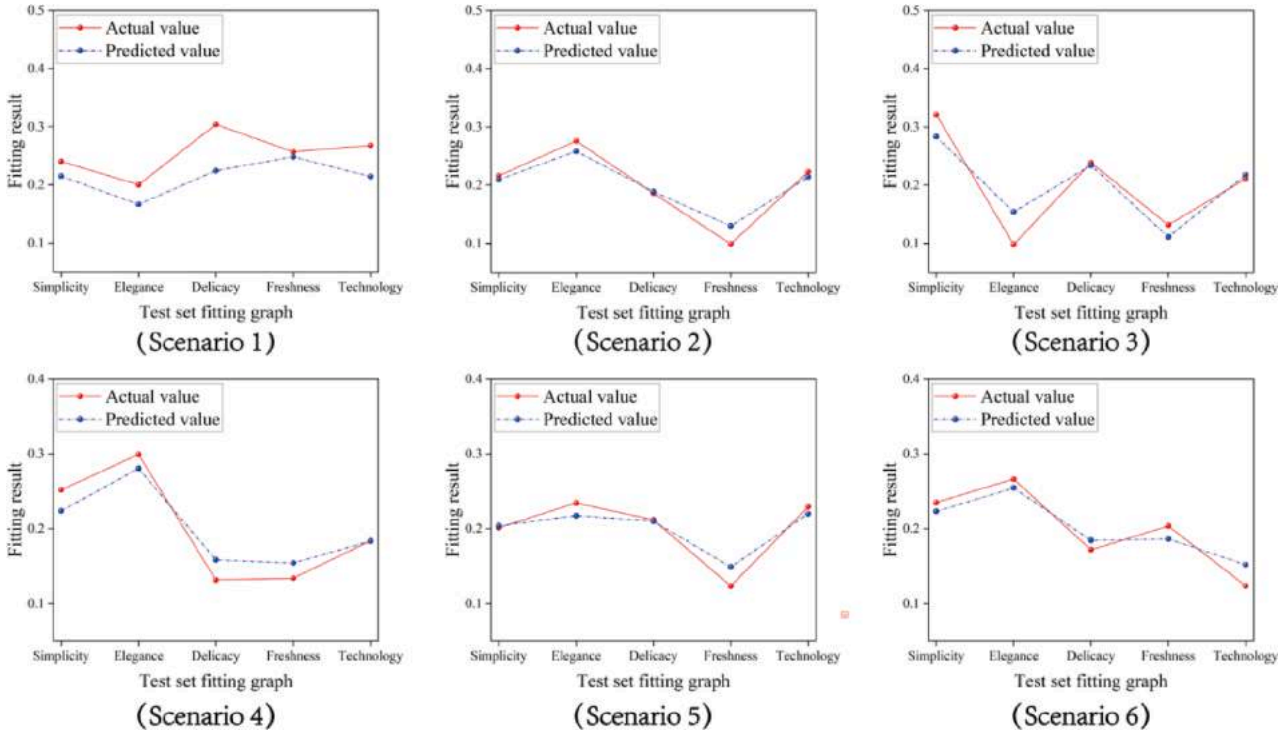

Fig. 19. Comparison between the actual user assessments and predictive value for the SSA-LSTM-Attention.

NEV-IC. Similarly, we trained mapping models for the remaining four users' emotional datasets (sense of elegance, sense of delicacy, sense of freshness and sense of technology). Then, the $9 \times 10 \times 10 \times 9 = 8100$ combinations of four morphological features were imported into the trained SSA-LSTM-Attention model for prediction, the emotional value of 8100 design combinations of NEV-IC were obtained. For emotional value of each combination, we weighted them with weights of emotional word from Table 7, and then summed them up. The final prediction yielded a maximum value of 9.43, corresponding to the decoded design element combination: $F_{(\max)} = \{4, 8, 8, 8\}$.

3.4. Analysis of design results

We analyzed the calculation results. In the table of morphological deconstruction, No. 4 center control panel, No. 8 screen, No.8 steering wheel, and No.8 instrument panel were taken as the reference objects to carry out the all-round design (Fig. 13). It should be noted that the computational results only provide a rough morphological reference for

the design of NEV-IC. In the actual design process, in addition to considering the morphological features derived from computation, it's essential to comprehensively consider five user emotions—simplicity, elegance, delicacy, freshness, and technology. Through the use of uniform color schemes and materials, overall consistency can be enhanced. Integrating multiple functions into a single interface or reducing the quantity of control elements can decrease complexity, thereby simplifying the control system and enhancing its sense of minimalism. Curves with a sense of streamline were introduced, the smooth lines can break the sense of rigidity, give the whole space an elegant atmosphere and enhance the sense of elegance. Materials with high quality are chosen, such as soft leather, aluminum alloy so as to enhance the sense of delicacy. The use of large areas of transparent materials, such as glass or transparent plastic, is helpful for introducing external light into the car, thus making the driver feel more fresh. A fully digital dashboard was adopted while integrating a large-size touch screen for controlling vehicle functions, entertainment systems, navigation and so on. The interface design should be clean and intuitive, supporting gesture control. This allows drivers to operate it easily and intuitively, enhancing the technological feel.

4. Discussion and evaluation

4.1. Machine learning models in emotional data prediction

A large number of studies have shown that machine learning models can be used to establish mapping models between morphological features and users' emotions, thus classifying and predicting users' emotions. We applied dataset to conventional machine learning models, including BPNN, SVR, and LSTM, and compared them with our proposed SSA-LATM-Attention model to evaluate their generalization ability and robustness. Firstly, we evaluated the performance of four models on the five datasets in the form of scatter plot (Fig. 14) and error band diagram (Fig. 15). In the scatter plot, the results of the training set and test set for the four models in different emotional data are presented in the form of linear fitting. BPNN showed poor performance on both the training and testing sets for the five emotional datasets. SVR and LSTM showed good performance on the training set but exhibited poor performance on the testing set. SSA-LSTM-Attention outperformed the other three models on both the training and testing sets. In the error band diagram of the test set, the error range of BPNN was significantly higher than that of other models in the five emotional datasets. The error range of SVR and LSTM were roughly the same. The error range of SSA-LSTM-Attention was obviously smaller than that of other models. Similarly, the evaluation coefficients (R^2 and RMSE) of the four models in the five emotional datasets were plotted in the same space (Fig. 16). The performance of SSA-LSTM-Attention was superior to the other types, both on the training and testing sets. It was shown that the introduction of SSA and Attention mechanism significantly reduced the prediction error of LSTM.

4.2. Evaluation of design scheme

In the evaluation stage, we selected the top 5 NEVs with the highest sales in 2023 using statistics data from STATISTA [76]. Subsequently, we engaged five design experts and twelve participants once again to evaluate the emotional aspects of six NEV-ICs (Fig. 17). It's noteworthy that scenario 1 serves as the output case study for this research. We presented the users' average value of five kinds of emotional evaluation in the form of radar chart (Fig. 18). The radar area of users' emotional evaluation in scheme 1 is the largest, which means that the design scheme produced by this study has the highest evaluation value, thus verifying the scientific and rational method proposed in this study. Concurrently, we deconstructed and encoded six NEV-ICs, extracting emotional prediction value using the SSA-LSTM-Attention model. Comparing predicted value with users' actual evaluations, the red line represents the actual evaluation value by the users for six samples, while the blue line represents the predicted value of SSA-LATM-Attention (Fig. 19). The results indicate that the SSA-LSTM-Attention model can effectively predict users' actual emotional responses when it confronted with new morphological data of NEV-IC.

5. Conclusion

The development of NEV contributes not only to environmental protection and sustainable development but also drives technological innovation and industrial upgrading, while simultaneously improving and enhancing energy utilization efficiency. The NEV-IC is not just about providing a comfortable driving environment, it also relates to user experience, safety, operability, and its impact on future modes of transportation. While some research has focused on identifying the emotional states of drivers to generate corresponding emotional feedback, there is still room for improvement in the emotional recognition and prediction for NEV-IC emotional design. Effectively predicting user emotion continues to be an area requiring exploration. As a pivotal tool in emotional design, KE can be applied to the design of NEV-IC. However, the challenge persists in establishing a more precise mapping model between user emotions and the morphological features of NEV-IC. To achieve emotionalization in the design of NEV-IC and establish a more accurate emotional prediction model, this study proposed a method for collecting morphological datasets with visual sequence features and an emotional prediction approach based on SSA-LSTM-Attention. In this paper, FA was used to reduce the dimensionality of collected emotional words, the core words were extracted as well. The morphological deconstruction table was used to summarize the component characteristics of the NEV-IC. Additionally, a dataset of NEV-IC morphology with visual sequence features was collected using eye-tracking technology and entropy-TOPSIS. The improved model of SSA-LSTM-Attention was used to fit the nonlinear relationship between users' emotions and morphological features. The optimal morphological combination for NEV-IC was ultimately predicted. In the program evaluation, the comprehensive scores of the NEV-IC design produced by us were higher than those of the existing representative programs in the market. Moreover, in the comparative experiment, we found that SSA-LSTM-Attention outperformed traditional machine learning models, such as BPNN, SVR, and LSTM, in user emotion prediction, thus validating the superiority of the proposed method in this study. This study can assist designers in understanding user emotional responses and producing product designs that align with users' emotional imagery, thereby stimulating their desire to purchase.

The contributions of this study are as follows:

1) The artificial intelligence technology is introduced to assist designers to make design decisions, which combines computer science and data science into the field of industrial design.
2) Combining eye-tracking technology with entropy-TOPSIS, we investigated the coupling between users' visual perception and professional designers' opinions, constructing a key morphological dataset with visual sequence features.
3) In this study, the LSTM is improved to promote the accuracy of data prediction. Compared to machine learning models widely applied in the field of KE, the improved model proposed in this study demonstrates superior performance.

However, there are still some limitations that need to be improved in this study:

1) The method proposed in this paper focuses on the study of products morphology. However, as for NEV-IC, intelligent materials, multimodal interaction and other aspects also affect users' emotions, so it is suggested to expand the research in the future.

2) Simple emotional words cannot accurately summarize users' emotions. In most cases, users' emotions are fuzzy and random. It is suggested that in future studies, physiological data can be collected by electroencephalography, picoelectricity, and other physiological detection techniques to measure users' emotions, thus improving the objectivity of data.
3) The method of NEV-IC emotional design in this study remains universally applicable. In future work, we will develop targeted design methods to enhance the performance of NEV-IC in user affective experiences.

CRediT authorship contribution statement

Nanyi Wang: Writing – review & editing, Writing – original draft, Formal analysis, Data curation. **Di Shi:** Software, Methodology. **Zengrui Li:** Visualization, Conceptualization. **Pingting Chen:** Writing – review & editing. **Xipei Ren:** Supervision, Funding acquisition, Conceptualization.

Declaration of competing interest

The authors declare that they have no known competing financial interests or personal relationships that could have appeared to influence the work reported in this paper.

Data availability

Data will be made available on request.

Acknowledgments

This work is supported by The National Social Science Fund of China (21CG192) and Ministry of Education of China's First Batch of New Humanities Research and Reform Practice Project (2021160005), All authors would also like to thank the anonymous referees for their constructive comments.

Appendix

Table A1
User emotional dataset.

Sample	Sense of simplicity	Sense of elegance	Sense of delicacy	Sense of freshness	Sense of technology
1	4.02	4.34	3.14	3.55	4.97
2	3.77	4.05	3.79	3.43	5.55
3	3.55	3.94	4.04	3.92	4.07
4	3.74	4.32	4.02	4.48	5.87
5	5.62	5.08	3.16	5.02	4.77
6	4.22	4.03	4.07	3.72	3.52
7	4.52	4.23	4.22	2.83	5.13
8	3.51	5.55	3.17	3.55	5.43
9	3.92	3.26	3.02	4.96	3.64
10	3.46	5.05	3.73	4.02	3.97
11	4.44	5.02	3.14	4.13	3.56
12	5.32	5.35	3.76	3.74	4.52
13	4.52	5.23	4.06	4.12	3.86
14	4.12	3.14	3.22	5.04	4.37
15	3.84	5.41	4.02	3.67	5.34
16	3.39	4.14	4.36	4.02	4.33
17	4.42	4.43	4.26	3.79	3.89
18	3.87	5.92	3.17	3.22	3.02
19	4.77	3.52	5.07	4.77	4.45
20	4.85	4.77	4.11	3.21	4.26
21	3.91	5.31	3.04	4.41	4.25
22	3.32	4.03	3.47	4.37	4.38
23	4.69	5.63	4.06	4.39	3.93
24	3.97	4.38	3.72	3.55	3.85
25	4.75	4.03	5.43	4.34	4.79
26	3.32	4.07	4.78	3.86	3.96
27	4.82	3.59	5.13	4.69	4.46
28	4.28	4.07	4.18	3.05	4.43
29	4.61	4.45	4.03	3.71	3.59
30	4.52	4.63	2.83	4.15	3.31
31	3.77	4.96	3.14	3.34	4.68
32	4.36	4.46	4.37	3.88	4.16
33	5.25	4.49	3.22	3.77	4.37
34	4.37	5.54	4.48	3.08	3.19
35	4.85	5.34	3.43	4.41	4.68
36	4.03	4.97	2.81	2.73	3.66
37	3.94	5.02	3.37	4.35	3.27
38	3.03	4.15	3.57	4.14	3.05
39	3.41	3.77	3.03	4.53	4.67
40	3.83	3.08	3.66	5.34	4.89
41	2.82	4.97	2.88	3.05	4.81
42	3.37	4.51	3.93	3.61	4.25
43	3.72	5.57	3.02	4.54	4.82
44	5.28	5.65	3.42	4.24	4.26
45	3.36	3.37	3.45	3.85	3.55
46	3.95	4.62	3.67	4.77	4.11
47	4.41	5.38	2.63	4.94	4.15
48	2.87	5.47	4.22	3.96	4.16

(*continued on next page*)

Table A1 (*continued*)

Sample	Sense of simplicity	Sense of elegance	Sense of delicacy	Sense of freshness	Sense of technology
49	3.63	4.48	3.63	4.26	3.88
50	3.48	4.12	4.57	3.92	3.67
51	4.34	5.02	3.32	3.96	3.68
52	3.32	3.73	2.89	4.35	4.58
53	4.37	4.92	3.06	5.36	4.09
54	4.61	3.97	4.23	2.67	4.12
55	4.57	4.71	4.67	2.93	3.69
56	4.71	5.37	4.26	2.15	3.62
57	4.67	5.15	3.55	4.49	5.27
58	4.75	5.13	4.54	2.18	4.26
59	4.17	4.58	4.32	5.14	4.45
60	4.61	3.03	4.63	2.58	3.68
61	5.28	5.35	3.37	4.34	4.55
62	4.58	5.14	3.14	3.85	3.17
63	4.73	5.29	4.03	3.68	4.48
64	3.65	5.02	3.93	4.79	3.88
65	3.99	4.31	4.52	5.12	5.13
66	4.05	4.97	4.38	2.43	3.98
67	3.12	5.19	3.31	4.47	4.04
68	5.08	5.14	3.72	3.61	4.34
69	3.56	4.93	3.66	3.28	4.79
70	3.35	5.48	3.76	3.44	4.02
71	5.11	5.05	3.82	2.66	3.62
72	5.96	4.62	3.11	3.91	4.23
73	5.88	4.58	3.12	3.87	4.11
74	4.17	3.87	4.38	2.87	4.01
75	3.78	3.04	3.33	5.68	4.57
76	5.04	4.32	4.13	2.91	4.46
77	3.23	3.62	4.39	3.16	4.05
78	2.82	5.18	2.88	3.04	4.81
79	4.23	5.96	4.22	3.47	5.26
80	5.42	4.49	3.32	3.69	4.52
81	4.65	3.74	4.43	3.25	4.53
82	4.45	5.02	3.77	4.45	5.87
83	3.07	4.16	3.52	5.23	4.05
84	4.17	3.87	4.39	2.88	4.02
85	4.33	4.37	2.17	5.12	3.69
86	3.64	2.48	3.72	4.45	4.74
87	4.17	3.88	4.38	2.88	4.01
88	4.59	5.62	4.05	3.66	4.07
89	4.78	4.53	3.86	4.13	3.65
90	4.34	3.38	3.05	4.09	4.21
91	4.52	5.36	3.89	2.92	3.98
92	4.07	4.87	4.33	3.45	4.84
93	4.83	4.78	4.02	3.09	3.62
94	4.29	4.79	2.75	4.01	3.97
95	4.84	3.39	4.32	3.17	3.85
96	2.93	5.23	2.74	4.22	4.02
97	4.59	5.64	3.99	4.38	3.91
98	4.06	3.35	3.97	4.46	4.32
99	4.45	3.06	3.45	5.09	3.88
100	4.42	4.35	4.68	3.68	4.93

Table A2
Dataset of morphological characterization.

Sample	Center control pane (F4)	Screen (F1)	Steering wheel (F3)	Instrument panel (F5)
1	1,0,0,0,0,0,0,0,0,0	0,1,0,0,0,0,0,0,0	0,0,1,0,0,0,0,0,0,0	0,0,0,1,0,0,0,0,0
2	1,0,0,0,0,0,0,0,0,0	0,1,0,0,0,0,0,0,0	0,1,0,0,0,0,0,0,0,0	0,0,0,0,1,0,0,0,0
3	0,0,0,0,0,0,0,1,0,0	0,0,0,0,0,1,0,0,0	0,0,0,0,0,0,0,1,0,0	0,0,0,0,0,0,0,0,1
4	1,0,0,0,0,0,0,0,0,0	0,0,0,0,0,0,0,1,0	0,0,0,0,0,0,0,1,0,0	0,0,0,0,1,0,0,0,0
5	0,0,0,1,0,0,0,0,0,0	0,1,0,0,0,0,0,0,0	0,0,0,0,0,0,0,1,0,0	0,0,0,1,0,0,0,0,0
6	0,0,0,0,0,0,1,0,0,0	0,0,0,0,0,1,0,0,0	0,0,0,0,0,0,0,0,1,0	0,0,0,0,0,0,1,0,0
7	1,0,0,0,0,0,0,0,0,0	0,1,0,0,0,0,0,0,0	0,0,0,0,0,1,0,0,0,0	0,0,0,0,0,1,0,0,0
8	1,0,0,0,0,0,0,0,0,0	0,1,0,0,0,0,0,0,0	0,0,0,0,0,0,0,1,0,0	0,1,0,0,0,0,0,0,0
9	0,0,0,0,0,0,0,1,0,0	0,0,0,0,0,1,0,0,0	0,1,0,0,0,0,0,0,0,0	0,0,0,1,0,0,0,0,0
10	0,0,0,0,0,0,0,0,0,1	0,0,0,0,1,0,0,0,0	0,0,0,0,0,0,0,1,0,0	0,1,0,0,0,0,0,0,0
11	0,0,0,0,0,0,0,1,0,0	0,1,0,0,0,0,0,0,0	0,0,0,1,0,0,0,0,0,0	0,0,0,0,0,0,0,0,1
12	0,0,0,1,0,0,0,0,0,0	0,1,0,0,0,0,0,0,0	0,1,0,0,0,0,0,0,0,0	0,0,0,0,1,0,0,0,0
13	0,0,0,0,0,0,0,0,1,0	0,0,0,0,0,0,1,0,0	0,0,0,0,0,1,0,0,0,0	1,0,0,0,0,0,0,0,0
14	0,0,0,0,0,1,0,0,0,0	1,0,0,0,0,0,0,0,0	0,0,0,0,0,0,1,0,0,0	0,0,0,1,0,0,0,0,0
15	1,0,0,0,0,0,0,0,0,0	0,1,0,0,0,0,0,0,0	0,0,0,0,0,0,0,1,0,0	0,1,0,0,0,0,0,0,0

(*continued on next page*)

Table A2 (*continued*)

Sample	Center control pane (F4)	Screen (F1)	Steering wheel (F3)	Instrument panel (F5)
16	0,0,1,0,0,0,0,0,0,0	0,1,0,0,0,0,0,0,0	0,0,0,0,0,1,0,0,0,0	1,0,0,0,0,0,0,0,0
17	0,0,0,0,0,0,1,0,0,0	0,0,0,0,0,1,0,0,0	0,0,0,0,0,0,0,1,0,0	0,0,0,0,0,0,1,0,0
18	0,0,0,0,0,0,0,0,1,0	0,0,0,0,1,0,0,0,0	0,1,0,0,0,0,0,0,0,0	0,1,0,0,0,0,0,0,0
19	0,0,0,0,0,0,1,0,0,0	0,0,0,0,0,0,0,1,0	0,0,0,0,0,1,0,0,0,0	0,0,0,0,0,1,0,0,0
20	0,1,0,0,0,0,0,0,0,0	0,1,0,0,0,0,0,0,0	0,0,0,0,0,0,0,1,0,0	0,0,0,0,0,1,0,0,0
21	0,1,0,0,0,0,0,0,0,0	0,1,0,0,0,0,0,0,0	0,0,0,0,0,1,0,0,0,0	0,0,0,0,1,0,0,0,0
22	0,0,0,0,1,0,0,0,0,0	1,0,0,0,0,0,0,0,0	0,0,0,0,0,0,1,0,0,0	1,0,0,0,0,0,0,0,0
23	0,0,0,0,0,0,0,0,1,0	0,0,1,0,0,0,0,0,0	0,0,0,0,0,0,0,1,0,0	0,0,0,0,0,0,0,1,0
24	0,0,0,0,0,0,0,1,0,0	0,0,0,0,0,1,0,0,0	0,1,0,0,0,0,0,0,0,0	0,0,0,0,0,0,1,0,0
25	0,0,0,0,0,0,1,0,0,0	0,0,0,0,0,0,0,1,0	0,0,0,0,0,0,0,1,0,0	0,0,0,0,0,1,0,0,0
26	0,0,1,0,0,0,0,0,0,0	0,1,0,0,0,0,0,0,0	0,0,0,0,0,0,0,0,0,1	0,0,0,0,1,0,0,0,0
27	0,0,0,0,0,0,1,0,0,0	0,0,0,0,0,0,0,1,0	0,0,0,0,0,1,0,0,0,0	0,0,0,0,0,1,0,0,0
28	0,0,0,0,0,0,0,0,1,0	1,0,0,0,0,0,0,0,0	0,0,1,0,0,0,0,0,0,0	1,0,0,0,0,0,0,0,0
29	0,0,0,0,0,0,1,0,0,0	0,0,0,0,0,1,0,0,0	0,1,0,0,0,0,0,0,0,0	0,0,0,0,0,0,1,0,0
30	0,1,0,0,0,0,0,0,0,0	0,0,1,0,0,0,0,0,0	0,0,0,0,0,0,0,1,0,0	1,0,0,0,0,0,0,0,0
31	1,0,0,0,0,0,0,0,0,0	0,1,0,0,0,0,0,0,0	0,0,0,0,0,1,0,0,0,0	1,0,0,0,0,0,0,0,0
32	0,0,0,0,0,0,1,0,0,0	0,0,0,0,0,1,0,0,0	0,0,0,0,0,0,0,1,0,0	0,0,0,0,0,0,1,0,0
33	0,0,0,1,0,0,0,0,0,0	0,1,0,0,0,0,0,0,0	0,0,1,0,0,0,0,0,0,0	0,0,0,1,0,0,0,0,0
34	0,0,0,0,0,0,0,0,1,0	0,0,0,0,1,0,0,0,0	0,0,0,0,1,0,0,0,0,0	1,0,0,0,0,0,0,0,0
35	0,1,0,0,0,0,0,0,0,0	0,1,0,0,0,0,0,0,0	0,1,0,0,0,0,0,0,0,0	0,0,1,0,0,0,0,0,0
36	0,1,0,0,0,0,0,0,0,0	0,1,0,0,0,0,0,0,0	0,0,1,0,0,0,0,0,0,0	0,0,0,0,0,0,0,0,1
37	0,1,0,0,0,0,0,0,0,0	0,1,0,0,0,0,0,0,0	0,1,0,0,0,0,0,0,0,0	0,1,0,0,0,0,0,0,0
38	0,0,0,0,1,0,0,0,0,0	0,0,0,0,1,0,0,0,0	0,0,0,1,0,0,0,0,0,0	0,1,0,0,0,0,0,0,0
39	0,0,0,0,1,0,0,0,0,0	1,0,0,0,0,0,0,0,0	0,0,0,0,0,0,1,0,0,0	1,0,0,0,0,0,0,0,0
40	0,0,0,0,0,1,0,0,0,0	1,0,0,0,0,0,0,0,0	0,0,0,0,0,0,0,1,0,0	0,0,0,1,0,0,0,0,0
41	1,0,0,0,0,0,0,0,0,0	0,1,0,0,0,0,0,0,0	1,0,0,0,0,0,0,0,0,0	1,0,0,0,0,0,0,0,0
42	0,0,1,0,0,0,0,0,0,0	0,1,0,0,0,0,0,0,0	1,0,0,0,0,0,0,0,0,0	1,0,0,0,0,0,0,0,0
43	0,1,0,0,0,0,0,0,0,0	0,1,0,0,0,0,0,0,0	1,0,0,0,0,0,0,0,0,0	0,0,1,0,0,0,0,0,0
44	0,1,0,0,0,0,0,0,0,0	0,1,0,0,0,0,0,0,0	0,0,0,1,0,0,0,0,0,0	0,0,1,0,0,0,0,0,0
45	0,0,0,0,0,0,1,0,0,0	0,0,0,0,0,1,0,0,0	0,0,0,0,0,0,0,0,1,0	0,0,0,0,1,0,0,0,0
46	0,0,0,0,0,0,0,1,0,0	0,0,0,0,0,1,0,0,0	0,0,0,0,0,1,0,0,0,0	0,0,0,0,0,0,1,0,0
47	0,1,0,0,0,0,0,0,0,0	0,1,0,0,0,0,0,0,0	0,0,0,0,0,0,0,1,0,0	0,0,0,1,0,0,0,0,0
48	0,0,0,0,1,0,0,0,0,0	0,1,0,0,0,0,0,0,0	0,0,0,0,1,0,0,0,0,0	0,1,0,0,0,0,0,0,0
49	0,0,0,0,0,0,0,0,0,1	0,0,0,0,0,0,1,0,0	0,0,0,0,0,0,0,0,1,0	0,1,0,0,0,0,0,0,0
50	0,0,0,0,0,1,0,0,0,0	0,0,0,0,0,1,0,0,0	0,0,0,0,0,0,0,0,0,1	0,0,0,0,0,0,1,0,0
51	0,0,0,0,0,0,0,0,0,1	0,0,0,0,0,0,1,0,0	0,0,0,0,0,0,1,0,0,0	1,0,0,0,0,0,0,0,0
52	0,0,0,0,1,0,0,0,0,0	1,0,0,0,0,0,0,0,0	0,0,0,0,0,0,1,0,0,0	1,0,0,0,0,0,0,0,0
53	0,0,0,0,0,0,0,1,0,0	0,1,0,0,0,0,0,0,0	0,1,0,0,0,0,0,0,0,0	0,0,0,1,0,0,0,0,0
54	0,1,0,0,0,0,0,0,0,0	0,1,0,0,0,0,0,0,0	0,0,1,0,0,0,0,0,0,0	0,0,0,0,0,1,0,0,0
55	0,0,0,0,0,0,1,0,0,0	0,0,0,0,0,1,0,0,0	0,0,0,0,1,0,0,0,0,0	0,0,0,0,0,0,1,0,0
56	0,0,0,0,0,0,0,0,1,0	0,0,0,1,0,0,0,0,0	0,0,0,0,1,0,0,0,0,0	1,0,0,0,0,0,0,0,0
57	0,1,0,0,0,0,0,0,0,0	0,1,0,0,0,0,0,0,0	0,0,0,0,0,0,0,1,0,0	0,0,1,0,0,0,0,0,0
58	0,0,0,0,0,0,0,0,1,0	0,0,0,1,0,0,0,0,0	0,0,0,0,1,0,0,0,0,0	0,0,0,0,1,0,0,0,0
59	0,0,0,0,0,0,1,0,0,0	0,0,0,0,0,0,0,1,0	0,1,0,0,0,0,0,0,0,0	0,0,0,0,1,0,0,0,0
60	0,0,0,0,0,1,0,0,0,0	0,0,0,0,0,0,0,0,1	0,0,0,0,0,0,0,0,1,0	0,0,0,0,0,1,0,0,0
61	0,1,0,0,0,0,0,0,0,0	0,1,0,0,0,0,0,0,0	0,0,0,1,0,0,0,0,0,0	0,0,1,0,0,0,0,0,0
62	0,1,0,0,0,0,0,0,0,0	0,0,0,0,0,1,0,0,0	0,1,0,0,0,0,0,0,0,0	0,0,0,0,0,0,1,0,0
63	0,0,0,0,0,0,0,0,1,0	0,0,1,0,0,0,0,0,0	0,0,0,0,0,0,0,1,0,0	0,0,0,0,1,0,0,0,0
64	0,0,0,0,0,0,0,0,0,1	0,0,0,0,0,0,1,0,0	0,0,0,0,0,0,0,0,1,0	0,1,0,0,0,0,0,0,0
65	0,0,0,0,0,0,1,0,0,0	0,0,0,0,0,0,0,1,0	0,0,0,0,0,0,0,1,0,0	0,0,0,0,1,0,0,0,0
66	0,0,0,0,0,0,0,0,1,0	0,0,0,1,0,0,0,0,0	0,0,1,0,0,0,0,0,0,0	0,1,0,0,0,0,0,0,0
67	0,0,0,0,0,0,0,1,0,0	0,0,0,0,0,1,0,0,0	1,0,0,0,0,0,0,0,0,0	0,0,0,0,0,0,1,0,0
68	0,0,0,1,0,0,0,0,0,0	0,1,0,0,0,0,0,0,0	0,0,0,0,0,0,1,0,0,0	0,1,0,0,0,0,0,0,0
69	1,0,0,0,0,0,0,0,0,0	0,1,0,0,0,0,0,0,0	0,0,0,0,0,0,0,0,0,1	0,0,0,0,1,0,0,0,0
70	0,0,0,0,0,0,0,0,1,0	0,0,0,1,0,0,0,0,0	1,0,0,0,0,0,0,0,0,0	0,1,0,0,0,0,0,0,0
71	0,0,0,0,0,0,0,0,1,0	0,0,0,1,0,0,0,0,0	0,0,0,1,0,0,0,0,0,0	1,0,0,0,0,0,0,0,0
72	0,0,0,1,0,0,0,0,0,0	0,0,0,0,0,0,0,0,1	0,0,0,0,0,1,0,0,0,0	0,0,0,0,1,0,0,0,0
73	0,0,0,1,0,0,0,0,0,0	0,0,0,0,0,0,0,0,1	0,0,0,0,0,1,0,0,0,0	0,0,0,0,1,0,0,0,0
74	0,0,0,0,0,0,1,0,0,0	0,0,0,0,0,1,0,0,0	0,0,1,0,0,0,0,0,0,0	0,0,0,0,0,0,1,0,0
75	0,0,0,0,0,1,0,0,0,0	1,0,0,0,0,0,0,0,0	0,0,0,0,0,1,0,0,0,0	0,0,0,1,0,0,0,0,0
76	0,0,0,1,0,0,0,0,0,0	0,1,0,0,0,0,0,0,0	1,0,0,0,0,0,0,0,0,0	0,0,0,0,0,1,0,0,0
77	0,0,1,0,0,0,0,0,0,0	0,0,0,0,1,0,0,0,0	0,0,0,0,0,0,0,1,0,0	1,0,0,0,0,0,0,0,0
78	1,0,0,0,0,0,0,0,0,0	0,1,0,0,0,0,0,0,0	1,0,0,0,0,0,0,0,0,0	1,0,0,0,0,0,0,0,0
79	0,0,0,0,0,0,0,0,1,0	0,1,0,0,0,0,0,0,0	0,0,0,0,0,0,0,1,0,0	0,0,0,0,1,0,0,0,0
80	0,0,0,1,0,0,0,0,0,0	0,1,0,0,0,0,0,0,0	0,0,1,0,0,0,0,0,0,0	0,0,0,1,0,0,0,0,0
81	0,0,0,0,0,0,0,1,0,0	0,0,0,1,0,0,0,0,0	0,0,0,0,0,0,0,1,0,0	0,0,0,0,0,1,0,0,0
82	0,0,0,0,0,0,0,1,0,0	0,1,0,0,0,0,0,0,0	0,0,0,0,0,0,1,0,0,0	0,0,1,0,0,0,0,0,0
83	0,0,0,0,1,0,0,0,0,0	1,0,0,0,0,0,0,0,0	0,1,0,0,0,0,0,0,0,0	0,1,0,0,0,0,0,0,0
84	0,0,0,0,0,0,1,0,0,0	0,0,0,0,0,1,0,0,0	0,0,1,0,0,0,0,0,0,0	0,0,0,0,0,0,1,0,0
85	0,1,0,0,0,0,0,0,0,0	0,0,0,0,0,1,0,0,0	0,1,0,0,0,0,0,0,0,0	0,0,0,1,0,0,0,0,0
86	0,0,0,0,0,1,0,0,0,0	1,0,0,0,0,0,0,0,0	0,0,1,0,0,0,0,0,0,0	0,0,0,1,0,0,0,0,0
87	0,0,0,0,0,0,1,0,0,0	0,0,0,0,0,1,0,0,0	0,0,1,0,0,0,0,0,0,0	0,0,0,0,0,0,1,0,0
88	0,0,0,0,0,0,0,0,1,0	0,0,0,0,0,1,0,0,0	0,0,0,0,0,1,0,0,0,0	0,0,0,0,0,0,1,0,0
89	0,1,0,0,0,0,0,0,0,0	0,0,0,1,0,0,0,0,0	0,0,0,0,0,0,1,0,0,0	0,0,0,1,0,0,0,0,0
90	0,0,0,0,0,0,0,1,0,0	0,0,0,1,0,0,0,0,0	0,0,1,0,0,0,0,0,0,0	0,0,0,1,0,0,0,0,0
91	0,0,0,0,0,0,0,0,1,0	0,0,0,1,0,0,0,0,0	0,0,0,0,0,0,1,0,0,0	0,1,0,0,0,0,0,0,0

(*continued on next page*)

Table A2 (*continued*)

Sample	Center control pane (F4)	Screen (F1)	Steering wheel (F3)	Instrument panel (F5)
92	1,0,0,0,0,0,0,0,0,0	0,0,0,0,0,0,0,1,0	0,0,0,0,1,0,0,0,0,0	1,0,0,0,0,0,0,0,0
93	0,1,0,0,0,0,0,0,0,0	0,1,0,0,0,0,0,0,0	0,1,0,0,0,0,0,0,0,0	0,0,0,0,0,1,0,0,0
94	0,1,0,0,0,0,0,0,0,0	0,1,0,0,0,0,0,0,0	0,0,1,0,0,0,0,0,0,0	0,0,0,1,0,0,0,0,0
95	0,0,0,0,0,0,0,1,0,0	0,0,0,1,0,0,0,0,0	0,1,0,0,0,0,0,0,0,0	0,0,0,0,0,1,0,0,0
96	0,0,0,0,0,0,0,1,0,0	0,1,0,0,0,0,0,0,0	1,0,0,0,0,0,0,0,0,0	0,0,0,0,0,0,0,0,1
97	0,0,0,0,0,0,0,0,1,0	0,0,1,0,0,0,0,0,0	0,0,0,0,0,0,0,1,0,0	0,0,0,0,0,0,0,1,0
98	0,0,0,0,0,1,0,0,0,0	1,0,0,0,0,0,0,0,0	0,0,0,0,1,0,0,0,0,0	0,0,0,1,0,0,0,0,0
99	0,0,0,0,0,1,0,0,0,0	1,0,0,0,0,0,0,0,0	0,0,0,1,0,0,0,0,0,0	0,0,0,1,0,0,0,0,0
100	0,0,0,0,0,0,0,1,0,0	0,1,0,0,0,0,0,0,0	0,0,0,0,0,0,0,1,0,0	0,0,0,0,0,1,0,0,0

References

[1] L. Nicoletti, S. Mayer, M. Brönner, et al., Design parameters for the early development phase of battery electric vehicles, World Electric Vehicle J. 11 (3) (2020) 47.

[2] H. Lin, X.L. Deng, D.S. Zhang, Taillight shape creative design based on generative adversarial networks, Comput.-Aided Des. Appl 20 (2023) 1043–1060.

[3] G. Sun, W. Zhuo, Research on optimization design of topology and size of the body structure for new energy vehicle, 2019 12th International Conference on Intelligent Computation Technology and Automation (ICICTA). IEEE, 2019: 104-107.

[4] P.K. Murali, M. Kaboli, R. Dahiya, Intelligent in-vehicle interaction technologies, Advanced Intelligent Systems 4 (2) (2022) 2100122.

[5] Y. Zhang, A. Carballo, H. Yang, et al., Perception and sensing for autonomous vehicles under adverse weather conditions: A survey, ISPRS J. Photogramm. Remote Sens. 196 (2023) 146–177.

[6] S. Hind, Dashboard design and the 'datafied'driving experience, Big Data Soc. 8 (2) (2021), 20539517211049862.

[7] S. Zepf, J. Hernandez, A. Schmitt, et al., Driver emotion recognition for intelligent vehicles: A survey, ACM Computing Surveys (CSUR) 53 (3) (2020) 1–30.

[8] X. Kang, Combining rough set theory and support vector regression to the sustainable form design of hybrid electric vehicle, J. Clean. Prod. 304 (2021) 127137.

[9] X. Lai, S. Zhang, N. Mao, et al., Kansei engineering for new energy vehicle exterior design: An internet big data mining approach, Comput. Ind. Eng. 165 (2022) 107913.

[10] Z. Liu, J. Wu, Q. Chen, et al., An improved Kansei engineering method based on the mining of online product reviews, Alex. Eng. J. 65 (2023) 797–808.

[11] X. Kang, S. Nagasawa, Integrating kansei engineering and interactive genetic algorithm in jiangxi red cultural and creative product design, J. Intell. Fuzzy Syst. Preprint (2023) 1–14.

[12] Z. Su, S. Yu, J. Chu, et al., A novel architecture: Using convolutional neural networks for Kansei attributes automatic evaluation and labeling, Adv. Eng. Inf. 44 (2020) 101055.

[13] Y. Gan, Y. Ji, S. Jiang, et al., Integrating aesthetic and emotional preferences in social robot design: An affective design approach with Kansei Engineering and Deep Convolutional Generative Adversarial Network, Int. J. Ind. Ergon. 83 (2021) 103128.

[14] H. Yadav, A. Thakkar, NOA-LSTM: An efficient LSTM cell architecture for time series forecasting, Expert Syst. Appl. 238 (2024) 122333.

[15] L. Peng, L. Wang, D. Xia, et al., Effective energy consumption forecasting using empirical wavelet transform and long short-term memory, Energy 238 (2022) 121756.

[16] W. An, L. Wang, D. Zhang, Comprehensive commodity price forecasting framework using text mining methods, J. Forecast. (2023).

[17] X. Yan, X. Gan, R. Wang, et al., Self-attention eidetic 3D-LSTM: Video prediction models for traffic flow forecasting, Neurocomputing 509 (2022) 167–176.

[18] T. Kong, W. Fang, P.E.D. Love, et al., Computer vision and long short-term memory: Learning to predict unsafe behaviour in construction, Adv. Eng. Inf. 50 (2021) 101400.

[19] S. Tsukiyama, M.M. Hasan, S. Fujii, et al., LSTM-PHV: prediction of human-virus protein–protein interactions by LSTM with word2vec, Brief. Bioinform. 22 (6) (2021) bbab228.

[20] Z.G. Deng, J. Lv, X. Liu, et al., Bionic design model for co-creative product innovation based on deep generative and BID, Int. J. Comput. Intelligence Syst. 16 (1) (2023) 8.

[21] Z. Chen, H. Xu, P. Jiang, et al., A transfer Learning-Based LSTM strategy for imputing Large-Scale consecutive missing data and its application in a water quality prediction system, J. Hydrol. 602 (2021) 126573.

[22] D. Chen, B. He, Y. Wang, et al., Prediction of Leakage Pressure during a Drilling Process Based on SSA-LSTM, Processes 11 (9) (2023) 2608.

[23] P. Jia, H. Chen, L. Zhang, et al., Attention-lstm based prediction model for aircraft 4-d trajectory, Sci. Rep. 12 (1) (2022) 15533.

[24] T. Wang, X. Sun, M. Zhou, et al., Construction of a novel production develop decision model based on text mined. International Conference on Human-Computer Interaction, Springer International Publishing, Cham, 2021, pp. 128–143.

[25] C. Yang, B. Yuan, J. Ye, A user-centered development model for innovation design in automated nursing beds, J. Adv. Mech. Design, Syst., Manuf. 17 (5) (2023) JAMDSM0062.

[26] H. Quan, S. Li, H. Wei, et al., Personalized product evaluation based on GRA-TOPSIS and Kansei engineering, Symmetry 11 (7) (2019) 867.

[27] X. Kang, Aesthetic product design combining with rough set theory and fuzzy quality function deployment, J. Intell. Fuzzy Syst. 39 (1) (2020) 1131–1146.

[28] S. Sheng, S. Zhiqiang, F. Xuan, et al., Research and Application of Color Factor Extraction Model for Military Cabins Based on Analytic Hierarchy Process, 2020 International Conference on Intelligent Design (ICID). IEEE, 2020: 67-74.

[29] T. Wang, M. Zhou, A method for product form design of integrating interactive genetic algorithm with the interval hesitation time and user satisfaction, Int. J. Ind. Ergon. 76 (2020) 102901.

[30] Y. Wang, S. Lu, D. Harter, Multi-sensor eye-tracking systems and tools for capturing Student attention and understanding engagement in learning: A review, IEEE Sens. J. 21 (20) (2021) 22402–22413.

[31] A.F. Klaib, N.O. Alsrehin, W.Y. Melhem, et al., Eye tracking algorithms, techniques, tools, and applications with an emphasis on machine learning and Internet of Things technologies, Expert Syst. Appl. 166 (2021) 114037.

[32] W. Yu, D. Jin, W. Cai, et al., Towards tacit knowledge mining within context: Visual cognitive graph model and eye movement image interpretation, Comput. Methods Programs Biomed. 226 (2022) 107107.

[33] T. Zheng, C.H. Glock, E.H. Grosse, Opportunities for using eye tracking technology in manufacturing and logistics: Systematic literature review and research agenda, Comput. Ind. Eng. 171 (2022) 108444.

[34] L. Jing, C. Tian, S. He, et al., Data-driven implicit design preference prediction model for product concept evaluation via BP neural network and EEG, Adv. Eng. Inf. 58 (2023) 102213.

[35] A.E. Ilhan, A. Togay, Use of eye-tracking technology for appreciation-based information in design decisions related to product details: Furniture example, Multimed. Tools Appl. (2023) 1–30.

[36] Y. Wang, S. Yu, N. Ma, et al., Prediction of product design decision Making: An investigation of eye movements and EEG features, Adv. Eng. Inf. 45 (2020) 101095.

[37] S.W. Hsiao, P.H. Peng, Y.C. Tsao, A method for the analysis of the interaction between users and objects in 3D navigational space, Adv. Eng. Inf. 50 (2021) 101364.

[38] O.R. Ogunseiju, N. Gonsalves, A.A. Akanmu, et al., Mixed reality environment for learning sensing technology applications in Construction: A usability study, Adv. Eng. Inf. 53 (2022) 101637.

[39] L. Mengtao, L. Fan, X. Gangyan, et al., Leveraging eye-tracking technologies to promote aviation safety-a review of key aspects, challenges, and future perspectives, Saf. Sci. 168 (2023) 106295.

[40] M. Wagner, P. Gröpel, K. Bibl, et al., Eye-tracking during simulation-based neonatal airway management, Pediatr. Res. 87 (3) (2020) 518–522.

[41] X. Xu, Z. Zhang, T. Long, et al., Mega-city region sustainability assessment and obstacles identification with GIS–entropy–TOPSIS model: A case in Yangtze River Delta urban agglomeration, China, J. Clean. Prod. 294 (2021) 126147.

[42] Y. Wang, Z. Wen, H. Li, Symbiotic technology assessment in iron and steel industry based on entropy TOPSIS method, J. Clean. Prod. 260 (2020) 120900.

[43] W. Huang, Y. Zhang, Y. Xu, et al., Urban rail transit passenger service quality evaluation based on the KANO–Entropy–TOPSIS model: the China case, Transport 37 (2) (2022) 98–109.

[44] Z. Wang, W. Liu, M. Yang, et al., A multi-objective evolutionary algorithm model for product form design based on improved SPEA2, Appl. Sci. 9 (14) (2019) 2944.

[45] L.Y. Ouyang, K.S. Chen, C.M. Yang, et al., Using a QCAC–Entropy–TOPSIS approach to measure quality characteristics and rank improvement priorities for all substandard quality characteristics, Int. J. Prod. Res. 52 (10) (2014) 3110–3124.

[46] H. Hewamalage, C. Bergmeir, K. Bandara, Recurrent neural networks for time series forecasting: Current status and future directions, Int. J. Forecast. 37 (1) (2021) 388–427.

[47] C. Avci, B. Tekinerdogan, C. Catal, Analyzing the performance of long short-term memory architectures for malware detection models, Concurrency and Computation: Practice and Experience 35 (6) (2023) 1.

[48] F. Landi, L. Baraldi, M. Cornia, et al., Working memory connections for LSTM, Neural Netw. 144 (2021) 334–341.

[49] R. Rouhi Ardeshiri, C. Ma, Multivariate gated recurrent unit for battery remaining useful life prediction: A deep learning approach, Int. J. Energy Res. 45 (11) (2021) 16633–16648.
[50] A. Kisvari, Z. Lin, X. Liu, Wind power forecasting–A data-driven method along with gated recurrent neural network, Renew. Energy 163 (2021) 1895–1909.
[51] R. Khaldi, A. El Afia, R. Chiheb, et al., What is the best RNN-cell structure to forecast each time series behavior? Expert Syst. Appl. 215 (2023) 119140.
[52] M.O. Turkoglu, S. D'Aronco, J.D. Wegner, et al., Gating revisited: Deep multi-layer RNNs that can be trained, IEEE Trans. Pattern Anal. Mach. Intell. 44 (8) (2021) 4081–4092.
[53] A. Sagheer, M. Kotb, Unsupervised pre-training of a deep LSTM-based stacked autoencoder for multivariate time series forecasting problems, Sci. Rep. 9 (1) (2019) 19038.
[54] J. Madiniyeti, Y. Chao, T. Li, et al., Concrete Dam Deformation Prediction Model Research Based on SSA–LSTM, Appl. Sci. 13 (13) (2023) 7375.
[55] A.M. Khedr, Z. Al Aghbari, P.P.V. Raj, MSSPP: modified sparrow search algorithm based mobile sink path planning for WSNs, Neural Comput. & Applic. 35 (2) (2023) 1363–1378.
[56] Y. Yue, L. Cao, D. Lu, et al., Review and empirical analysis of sparrow search algorithm, Artif. Intell. Rev. 56 (10) (2023) 10867–10919.
[57] J. Li, J. Chen, J. Shi, Evaluation of new sparrow search algorithms with sequential fusion of improvement strategies, Comput. Ind. Eng. 182 (2023) 109425.
[58] P. Kathiroli, K. Selvadurai, Energy efficient cluster head selection using improved Sparrow Search Algorithm in Wireless Sensor Networks, J. King Saud Univ.-Comput. Inform. Sci. 34 (10) (2022) 8564–8575.
[59] P. Chen, H. Wang, H. Yan, et al., sEMG-based upper limb motion recognition using improved sparrow search algorithm, Appl. Intell. 53 (7) (2023) 7677–7696.
[60] J. Gai, K. Zhong, X. Du, et al., Detection of gear fault severity based on parameter-optimized deep belief network using sparrow search algorithm, Measurement 185 (2021) 110079.
[61] I.H. Sarker, Deep learning: a comprehensive overview on techniques, taxonomy, applications and research directions, SN Computer Science 2 (6) (2021) 420.
[62] M.H. Guo, T.X. Xu, J.J. Liu, et al., Attention mechanisms in computer vision: A survey, Computational Visual Media 8 (3) (2022) 331–368.
[63] M. Li, Y. Wang, Z. Wang, et al., A deep learning method based on an attention mechanism for wireless network traffic prediction, Ad Hoc Netw. 107 (2020) 102258.
[64] Q. Ren, M. Li, H. Li, et al., A novel deep learning prediction model for concrete dam displacements using interpretable mixed attention mechanism, Adv. Eng. Inf. 50 (2021) 101407.
[65] Y. Xie, R. Liang, Z. Liang, et al., Speech emotion classification using attention-based LSTM, IEEE/ACM Trans. Audio Speech Lang. Process. 27 (11) (2019) 1675–1685.
[66] Y. Cao, Y. Ding, M. Jia, et al., A novel temporal convolutional network with residual self-attention mechanism for remaining useful life prediction of rolling bearings, Reliab. Eng. Syst. Saf. 215 (2021) 107813.
[67] J. Qiu, B. Wang, C. Zhou, Forecasting stock prices with long-short term memory neural network based on attention mechanism, PLoS One 15 (1) (2020) e0227222.
[68] G. Liu, J. Guo, Bidirectional LSTM with attention mechanism and convolutional layer for text classification, Neurocomputing 337 (2019) 325–338.
[69] M. Lin, J. Wu, J. Meng, et al., State of health estimation with attentional long short-term memory network for lithium-ion batteries, Energy 268 (2023) 126706.
[70] DeCoster J. Overview of factor analysis. 1998.
[71] C. Yang, F. Liu, J. Ye, A product form design method integrating Kansei engineering and diffusion model, Adv. Eng. Inf. 57 (2023) 102058.
[72] V. Čok, D. Vlah, J. Povh, Methodology for mapping form design elements with user preferences using Kansei engineering and VDI, J. Eng. Des. 33 (2) (2022) 144–170.
[73] X. Liu, S. Yang, Study on product form design via Kansei engineering and virtual reality, J. Eng. Des. 33 (6) (2022) 412–440.
[74] S. Khullar, N. Singh, Water quality assessment of a river using deep learning Bi-LSTM methodology: forecasting and validation, Environ. Sci. Pollut. Res. 29 (9) (2022) 12875–12889.
[75] N.M. Shahani, M. Kamran, X. Zheng, et al., Predictive modeling of drilling rate index using machine learning approaches: LSTM, simple RNN, and RFA, Pet. Sci. Technol. 40 (5) (2022) 534–555.
[76] https://www.statista.com/statistics/960121/sales-of-all-electric-vehicles-worldwide-by-model/.